EXAMENSARBETE INOM ELEKTROTEKNIK,
AVANCERAD NIVÅ, 30 HP

STOCKHOLM, *SVERIGE 2019*

Non-destructive Evaluation of Ultrasound Contrast Agent

Icke-destruktiv utvärdering av ultraljudskontrastmedel

WENDI LÖFFLER

KTH
SKOLAN FÖR ARKITEKTUR OCH SAMHÄLLSBYGGNAD

Abstract

Clinical ultrasound imaging techniques can be greatly improved by the use of ultrasound contrast agents (UCAs). While microbubbles (MBs) without shell are unstable and cannot be used for practical applications, a shell produced from biocompatible polyvinylalcohol (PVA) significantly improves chemical versatility and stability. The oscillation characteristics of a UCA are strongly dependent on concentration, applied pressure and viscoelastic parameters of the shell. Modifications in the shell as incorporation of antibodies or targeted molecules affect the bubble oscillation and resonance frequency of the MB suspension. In this presented work a tool for systematic characterization of UCAs is developed. Linear acoustic behaviour of PVA shelled MBs is examined. The acoustic driving pressure is kept below 100 kPa. The MB concentration is $1{\cdot}10^6\,\mathrm{ml}^{-1}$. Attenuation and phase velocity profiles of ultrasound waves propagating through the UCA are measured using six narrow-band single crystal transducers that cover a frequency range between 1 and 15 MHz. The oscillation of a single bubble is modeled as a linear oscillator adapting HOFF's model suitable for all shell thicknesses. The suspension is modeled through superposition of single bubbles. Knowing all parameters the resonance frequency of a MB suspension can be predicted. The model is fitted to experimental data to determine the viscoelastic shell parameters. The shell thickness is challenging to determine exactly and assumed to be either proportional to the outer shell radius or constant. Assuming a proportional shell thickness the calculated resulting shell parameters were shear modulus $G_s = 14.5\,\mathrm{MPa}$, shear viscosity $\eta_s = 0.322\,\mathrm{Pa{\cdot}s}$ and shell thickness $d_s = 16\,\%$ of the outer radius. When instead assuming a constant shell thickness the determined parameters were in similar order of magnitude. Resonance frequency of the suspension was determined to 11.6 MHz. The developed tool can be used to characterize MBs with a modified shell independently of shell thickness and to predict resonance frequency of gas or air filled UCAs with known shell parameters.

Sammanfattning

Kliniska ultraljud bildgivningstekniker kan förbättras kraftigt genom användning av ultraljudkonstrastmedel (ultrasound contrast agents (UCAs)). Mikrobubblor (microbubbles (MBs)) utan skal är instabila och kan inte användas i klinik, men stabiliteten och mångsidigheten kan betydligt förbättras genom att täcka bubblorna med ett skal av t.ex. polyvinylalcohol (PVA). Oscilleringsegenskaper av UCAs är starkt beroende av koncentrationen, använt tryck och de viskoelastiska parametrarna av skalet. Förändringar i skalet som t.ex. inkorporation av antikroppar eller målriktade molekyler påverkar oscilleringen av bubblorna och resonansfrekvensen av vätskeblandningen. I detta arbete utvecklas ett vertyg för att systematiskt kunna utvärdera UCAs. Det linjära akustiska beteendet av MBs med skal av PVA utvärderas här när den akustiska drivkraften hålls under 100 kPa och koncentrationen av MBs i suspensionen är $1 \cdot 10^6\,\mathrm{ml}^{-1}$. Dämpning- och fashastighetsprofilerna av ultraljudvågor som utbreder sig i kontrastmedlet mäts med sex singelkristall smalbandstransducrar som avbildar i frekvensband mellan 1 och 15 MHz. Suspensionen modeleras genom att anpassa HOFF's ansats så att MBs kan modeleras oberoende av skaltjockleken. Resonansfrekvensen av en MB suspension kan genom framtaget verktyg förutsägas om alla parametrar är kända. Modellen anpassas till experimentella data för att bestämma de viskoelastiska skalparametrarna. Tjockleken av skalet är utmanande att exakt bestämma och antas vara antingen proportionell till den yttre skalradien eller konstant. För en proportionel skalradie resulterar modellen i: skjuvmodul $G_s = 14.5\,\mathrm{MPa}$, viskositet $\eta_s = 0.322\,\mathrm{Pa{\cdot}s}$ och skaltjocklek $d_s = 0.16\,\%$ av yttre skalradius. Antas istället att skaltjockleken är konstant är resultatet liknande. Resonansfrekvensen av suspensionen bestäms därefter till 11.6 MHz. Verktyget kan således användas för att karakterisera MBs med modifierat skal oberoende av skaltjockleken och för att förutsäga resonansfrekvensen av gas- och luftfyllda UCAs med kända skalparametrar.

Contents

1 Introduction **1**
1.1 Aim of study 2

2 Theoretical Approach **4**
2.1 Mathematical Modeling of a single microbubble oscillation 5
2.1.1 Components of the oscillator 6
2.2 Speed of sound in the microbubble suspension 8

3 Experimental Methods **11**
3.1 Experimental Setup 11
3.1.1 Transducer range 12
3.1.2 Sensitivity of transducers 13
3.1.3 Microbubble suspension and particle size distribution 14
3.2 Data processing 15
3.2.1 Ambiguities in handling phase information 15

4 Post processing **17**
4.1 Measures for the goodness of fit 17
4.2 Rank-based algorithm 18

5 Results **19**
5.1 Experimental 19
5.2 Simulation 19
5.2.1 Simulation parameters 20
5.2.2 Simulation results 21

6 Discussion **27**

7 Conclusion and Future Work **30**

Bibliography **32**

A Literature Review **38**
A.1 The use of ultrasound contrast agents 38
A.1.1 Microbubbles as ultrasound contrast agent 38
A.1.2 Composition of microbubbles 39
A.2 Physical properties of the ultrasound beam 40
A.3 Acoustic behaviour of microbubbles in the ultrasonic field 41
A.3.1 Dependence on signal properties and the linear regime 43
A.3.2 Dependence on bubble and shell properties 43
A.3.3 Radiation force 44
A.4 Acoustic bubble characterization 44
A.4.1 Attenuation 45
A.4.2 Phase velocity 46
A.5 Theoretical description of the bubble behaviour 48
A.5.1 Modified Rayleigh-Plesset equation 48
A.5.2 The microbubble as linear oscillator 49
A.5.3 Modeling of coated microbubbles 50
A.6 Resonance frequency of microbubbles 51
A.6.1 Types of bubble oscillations and their influence on the resonance frequency 52

B Measures of Goodness **54**

Acronym

UCA	ultrasound contrast agent
MB	microbubble
US	ultrasound
PVA	polyvinylalcohol
MI	mechanical index
STFT	short time Fourier transform
TOF	time of flight
FFT	fast Fourier transform
BW	band width
NFL	near field length
MSE	Mean squared error

List of symbols

Symbol	Meaning	Unit
a	bubble radius of shell free bubble	m
a_1, a_2	inner and outer shell radius	m
A_b	bubble surface	m^2
c	phase velocity in bubbly liquid	$\mathrm{m/s}$
c_L	speed of sound in surrounding liquid	$\mathrm{m/s}$
c_w	speed of sound in water	$\mathrm{m/s}$
C_a	cross correlation of attenuation	
C_p	cross correlation of phase velocity	
d_s	shell thickness	m
f_0	resonance frequency	Hz
f_l, f_h	lower and higher cut-off frequency	Hz
f_c	center frequency	Hz
f_p	peak frequency	Hz
F_M, F_S, F_R	forces acting on the components of the oscillator	N
F_r	friction force	N
G_s	shear modulus	Pa
H	Displacement transfer function	
k_c	complex wave number in MB suspension	m^{-1}
k_L	wave number in the surrounding liquid	m^{-1}
K	complex bulk modulus of bubbly liquid	Pa
K_b	bulk modulus of single bubble	Pa
K_L	bulk modulus of liquid	Pa
L	Length of the specimen	m
M	mass	kg
M_L	mass of surrounding liquid	kg
M_{gas}	mass of the gas inside the bubble	kg
M_s	mass of the shell	kg
n	number of bubbles	
p_0	atmospheric pressure	Pa
$p_i(t)$, $\hat{p}_i(\omega)$	acoustic driving pressure	Pa
p_g	gas pressure inside the bubble	Pa
$p_s(r)$	radiated pressure field	Pa
$P_{xx,ref}$	Power spectrum of reference signal	V^2
R, R_c, $R_{\eta,L}$, $R_{\eta,S}$	damper	$\mathrm{kg/s}$
S	stiffness	$\mathrm{Pa} \cdot \mathrm{m}$
$s_{ref}(t)$, $\hat{s}_{ref}(\omega)$	reflected signal from water	V
$s_{MB}(t)$, $\hat{s}_{MB}(\omega)$	reflected signal from MB suspension	V
T_1, T_2, $T_L(r)$	Radial stress across the shell	Pa
$u + jv$	complex speed of sound ratio	
Z_m	mechanical impedance	$\mathrm{kg/s}$

Symbol	Meaning	Unit
α	attenuation	$\mathrm{db/cm}$
δ	damping ratio	
Δf_{max}	difference in maximum	Hz
η_s	shear viscosity	$\mathrm{Pa \cdot s}$
κ	polytropic gas exponent	
$\xi(t)$, $\hat{\xi}(\omega)$	radial displacement	m
ρ	density of bubbly liquid	$\mathrm{kg/m^3}$
ρ_L	density of the liquid	$\mathrm{kg/m^3}$
ρ_s	density of the shell	$\mathrm{kg/m^3}$
ϕ_{MB}	phase of signal from MB suspension	
ϕ_{ref}	phase of reference signal	
ω_0	angular resonance frequency	Hz

Chapter 1

Introduction

Ultrasound imaging is widely used in clinical practice as it is an inexpensive, non-invasive and real time imaging technique [1]. ultrasound contrast agents (UCAs) have been in use for image enhancement of tissue and blood vessels for some decades, mostly using micro sized gas bubbles confined by lipid or polymer shell [2]. Instead of using the former common and well characterized lipid shelled MBs, CAVALIERI et al [3] proposed usage of a biocompatible polyvinylalcohol (PVA) shell. This improves both mechanical stability and shelf life time of the bubbles, but as well allows easier binding and delivering of drugs and nanoparticles [4]. Driving the UCA at resonance frequency offers several advantages in clinical practice. Maximum oscillation of MBs is achieved and thus highest scattering and highest efficiency, but also maximum release of drugs when incorporated into the body [5]. More information about composition of the MBs can be found in appendix A.1 and about effects in usage of resonance frequencies is described in appendix A.6.

Experimental characterization has been conducted using both optical and acoustical methods (see appendix A.4), gaining information about bubble oscillation and acoustic characteristics. However, when doing experimental characterization the viscoelastic parameters of the shell remain generally unknown. That is, a theoretical model of the UCA needs to be developed including characteristics of the shell as shear modulus and shear viscosity. The viscoelastic parameters are acquired by fitting the modeled data to the experimentally gaining knowledge about the coefficients attenuation and phase velocity (see appendix A.3).

Models to describe oscillations of coated MBs have been set up by several authors mostly using the modified Rayleigh-Plesset equation [6] as base (see appendix A.5.3), e.g. by FRINKING and DE JONG [7], MARMOTTANT et al [8] or SARKAR et al [9]. The models are mainly applicable to describe lipid shelled bubbles and assume that the shell thickness $d_s < 5\,\%$ of the outer bubble radius.

PVA coated bubbles as designed by TORTORA et al [10] have a shell that is thick compared to the bubble radius. CHURCH et al [11] modified the Rayleigh-Plesset equation to derive non-linear equations of motion for the bubble making no prior assumption on the shell thickness. GRISHENKOV et al [12] applied a linearized version of the CHURCH model to characterize three types of PVA shelled MB. The model is adjusted to include frequency dependent viscoelastic shell parameters for a shell assumed to be thick ($\gg 5\,\%$) compared to the bubble radius. Acoustic behaviour of the bubble in the frequency range between 3 and 13 MHz was investigated using one broadband transducer with center frequency $f_c = 10\,\mathrm{MHz}$ offering a high accuracy of the experimental data around f_c. To receive high accuracy also in lower frequency range, additional transducers are needed.

HOFF et al [13] extensively characterized MB oscillations modeling a single MB as linear oscillator. Viscoelastic parameters are determined for three contrast agents stabilized by thin polymeric shells in the frequency range between 1 and 8 MHz. Early in the derivation the assumption of thin shell is introduced in his work.

1.1 Aim of study

In the presented work a procedure is developed to characterize UCAs of different concentration and type quickly, easy and repeatable. For acquisition of shell parameters and information about resonance both experimentally gathered information and a theoretical model of the MB suspension are needed. The model fitted to the experimental data provides the desired parameters and offers deeper understanding of the MB oscillation. The process is schematically presented in fig. 1.1.

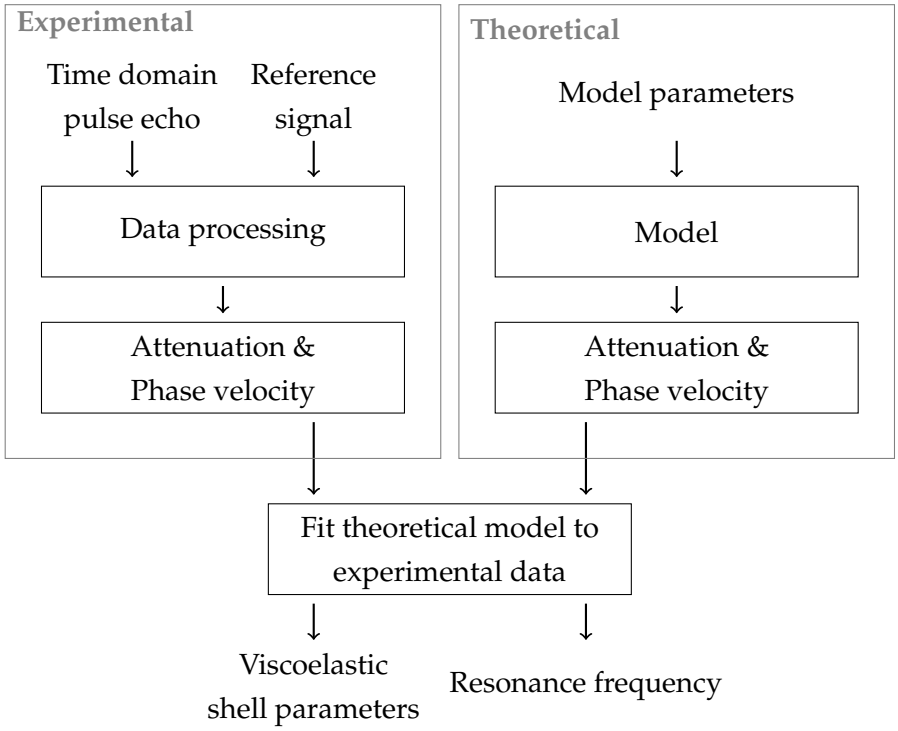

Figure 1.1: Schematic representation of the work process

Linear acoustic properties are investigated in the frequency range between 1 and 15 MHz using six single crystal narrow-band transducers to gain the profiles for attenuation and phase velocity (see chapter 3). HOFF's model is adjusted and combined with CHURCH to be suitable for thick shelled MBs (see chapter 2). The viscoelastic parameters are assumed to be constant and acquired by fitting modeled to experimental data (see chapter 4 and chapter 5). Therefore, both attenuation and phase velocity curve are considered in the same procedure using a rank-based algorithm to avoid ambiguities in the calculated characteristics.

Chapter 2

Theoretical Approach

In the following chapter, a theoretical approach to model linear oscillations of the MB suspension is given. Each bubble is modeled individually and resonance frequency and damping ratio of the single bubble are determined. To acquire the characteristics of the suspension single bubble oscillations are superposed. Superposition is possible because of the Waterman-Truel condition that is explained in appendix A.5.
The approach is derived based on HOFF et al [14]. It is modified to overcome the thin-shell-assumption done by HOFF. Attenuation and phase velocity curves are simulated using the model derived in this chapter. The concept of attenuation and phase velocity is explained in appendix A.4.
A schematic representation of a coated MB is presented in fig. 2.1.

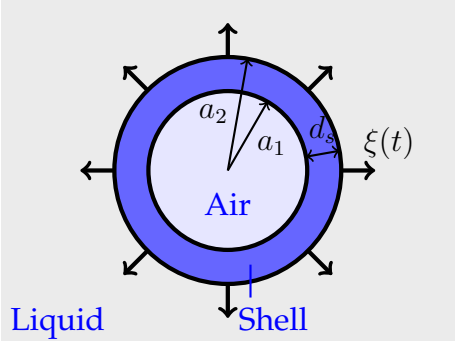

Figure 2.1: Schematic representation of a coated MB

The outer shell radius a_2 varies with time under ultrasound pressure. Shell thickness d_s is assumed to be either constant or propor-

tional to a_2. The inner bubble radius is $a_1 = a_2 - d_s$. The bubble is filled with air and coated by a polymer shell as described in appendix A.3.2. The surrounding liquid is water.

2.1 Mathematical Modeling of a single microbubble oscillation

A single bubble can be considered as a mechanical linear oscillator as presented in fig. 2.2.

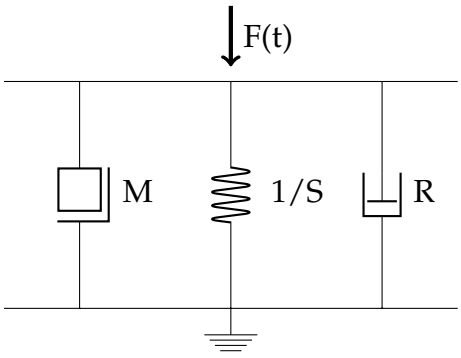

Figure 2.2: One bubble modeled as linear oscillator

The spring S represents the gas pressure inside the bubble, the mass M is the dynamic mass of the bubble and the damper R corresponds to damping due to viscosity of liquid and shell and radiation of sound. The equation of motion for the linear oscillator is as follows

$$F_M + F_R + F_S = F_i(t) = \int_A p_i(t) dA_b \tag{2.1}$$

with $p_i(t)$ being the driving acoustic pressure. F_m, F_R and F_S are the forces acting on the oscillator components. S is the bubble surface and due to the spherical shape solved to $S = 4\pi a_2$. When assuming the MB to act in the linear regime motion of the bubble surface can be linearized as follows:

$$a(t) = a_e + \xi(t) \tag{2.2}$$

with a_e being the initial bubble radius and $\xi(t)$ the radial displacement. The equation of motion can then be rewritten as

$$M\ddot{\xi} + R\dot{\xi} + S\xi = -4\pi a_2^2 \cdot p_i \tag{2.3}$$

That is similar to the linearized version of the Rayleigh-Plesset equation explained in appendix A.5.2.
Resonance frequency f_0 and damping ratio δ of the single bubble can be calculated from the components of the linear oscillator as follows:

$$\omega_0^2 = \frac{s}{M} \tag{2.4}$$

$$f_0 = \frac{1}{2\pi}\sqrt{\frac{S}{M}} \tag{2.5}$$

$$\delta = \frac{R}{\omega_0 M} \tag{2.6}$$

where ω_0 is the angular frequency.

2.1.1 Components of the oscillator

In the following formulas for calculation of stiffness S, dynamic mass M and damping constants R are derived.

Stiffness

Stiffness in the model is a combination of gas pressure inside the bubble and stiffness of the shell. Following HOFF [14] the stiffness of an uncoated bubble is as follows:

$$S_{uncoated} = 12\pi a_2 \kappa p_0 \tag{2.7}$$

with κ being the polytropic gas exponent and p_0 the atmospheric pressure. To account for the shell, the radial stress across the shell $T_2 - T_1$needs to be considered and included into the derivation of the stiffness. The stress difference is resolved by HOFF to

$$T_2 - T_1 = 12 G_s \frac{d_s}{a_2^2} \cdot \xi \tag{2.8}$$

The radial stress in liquid is $T_L(r)$ and the gas pressure inside the bubble is p_g. the boundary conditions for the stress difference are then:

$$T_2 = T_L(a_2) \tag{2.9}$$

$$T_1 = -p_g \tag{2.10}$$

$$\Rightarrow T_L = (T_2 - T_1) - p_g \tag{2.11}$$

The force from the shelled bubble acting on the liquid F_s is then T_L integrated over the bubble surface:

$$F_s = -\int\int_S T_L dS = -4\pi a^2 T_L = -(12\pi a \kappa p_0 + 48\pi G_s d_s) \tag{2.12}$$

Applying Hooke's law the spring constant s is:

$$s = 12\pi a_2 \kappa p_e + 48\pi G_s d_s \tag{2.13}$$

The first part of the equation is equal to the stiffness without shell, the second part accounts for the shell stiffness.

Inertia

Inertia is introduced into the system through motion of the liquid surrounding the bubble as well as the mass of the bubble [14]:

$$M = M_L + M_{gas} + M_{Shell} \tag{2.14}$$

with M_L being the mass of the surrounding liquid set in motion by bubble oscillations, M_{gas} the mass of the gas inside the bubble and M_S the mass of the shell. The contribution of the gas weight can be neglected, since gas density is much smaller liquid density. M_L is derivated from the pressure field p_s radiated from the oscillating bubble, which is for a diverging spherical wave

$$p_s(r) = p_s(a_2)\frac{a_2}{r} \cdot e^{j(\omega t - k_c r)}. \tag{2.15}$$

M_L is then calculated from the mechanical impedance Z_m at bubble surface:

$$F_M = -Z_m \dot{\xi} = -(R + j\omega M)\dot{\xi} \tag{2.16}$$

$$F_M = -4\pi a_2^2 p_s = -4\pi a_2^3 \rho_L (k_c a_2 + j)\dot{\xi} \tag{2.17}$$

$$\Rightarrow M_L = 4\pi a_2^3 \rho_L \tag{2.18}$$

where ρ_L is the density of the surrounding liquid and k_c the complex wave number.
The mass of the shell is calculated as

$$M_S = \pi(a_2^2 - a_1^2)\rho_S \tag{2.19}$$

The summation yields

$$M = 4\pi a_2^3 \rho_L + \pi(a_2^2 - a_1^2)\rho_S \tag{2.20}$$

which is the inertia constant for the PVA shelled MB that is to be modeled.

Damping

Different effects introduce damping to the bubble oscillation. Radiation resistance R_c represents energy loss through sound radiation. Both the surrounding liquid and the shell introduce a damping term depending on their viscosity (R_L and R_S). The damping constant is the sum of all damping contributions:

$$R = R_c + R_{\eta,L} + R_{\eta,S} \tag{2.21}$$

Damping due to radiation resistance is related to the mechanical impedance through $Z_m = R_c + j\omega m$ which resolves to

$$R_c = Re\{Z_m\} = 4\pi a_2^2(\rho_L c_w(k_c a_2)^2) \tag{2.22}$$

Note that radiation resistance depends only on liquid and on the motion of the bubble surface and is thus independent of the shell.
Liquid viscosity introduces damping to the bubble oscillation. The viscous damping term is derivated from the friction force $F_r = -R\dot{\xi}$ following CHURCH et al [11] to

$$R_{\eta,L} = \beta M a_1^3 \eta_L \omega_0 \tag{2.23}$$

where β is a constant factor:

$$\beta = 4 \cdot \left[\rho_S a_1^2 \Big(1 + \frac{\rho_L - \rho_S}{\rho_S}\Big)\frac{a_1}{a_2}\right]^{-1}. \tag{2.24}$$

Shell viscosity is also derived from the friction force considering the radial stress difference:

$$R_{\eta,s} = \beta m V_s \eta_s \omega_0 \tag{2.25}$$

with $V_s = a_2^3 - a_1^3$. Note that R_c is frequency dependent whereas $R_{\eta,L}$ and $R_{\eta,S}$ are constant.

2.2 Speed of sound in the microbubble suspension

In the precious section the model for a single MB was explained. In the following section all bubbles are considered to resolve the model

for attenuation and phase velocity curve of the MB suspension.
The incoming ultrasound wave is a plane harmonic wave with the complex wavenumber k_c. Knowledge of k_c yields attenuation and phase velocity curves. This is further explained in appendix A.2. The complex wave number is given as $k_c(\omega) = k_r + jk_i$. This is related to the speed of sound in the suspension c_c and in surrounding liquid c_L through

$$k_c = \frac{\omega}{c_c} \tag{2.26}$$

$$k_L = \frac{\omega}{c_L} \tag{2.27}$$

with k_L being the wave number of the ultrasound signal in water. Define the ratio of speed of sound by introduction of a complex number $u + jv$:

$$\frac{c_L}{c_c} = u + jv \tag{2.28}$$

The wave numbers are thus related as

$$k_c = k_L \cdot (u + jv) \tag{2.29}$$

Through Fourier transformation of the equation of motion, eq. (2.3), the radial displacement function can be derived in frequency domain:

$$\hat{\xi}(\omega) = \frac{1}{\rho_L a_2 \omega_0^2} \cdot \frac{\hat{p}_i(\omega)}{\left(\frac{\omega}{\omega_0}\right)^2 - 1 - j\frac{\omega}{\omega_0}\delta}. \tag{2.30}$$

By division between radial displacement and sound pressure a radial displacement transfer function is defined:

$$H\left(\frac{\omega}{\omega_0}\right) = \rho_L a_2 \omega_0^2 \frac{\hat{\xi}(\omega)}{\hat{p}_i(\omega)} \tag{2.31}$$

$$= \frac{1}{\frac{\omega}{\omega_0}^2 - 1 - j\frac{\omega}{\omega_0}\delta} \tag{2.32}$$

with $H(\frac{\omega}{\omega_0})$ being a complex valued function.
Using the bulk modulus K and density of the bubbly liquid ρ, COMMANDER & PROSPERETTI [15] derived the speed of sound in a bubbly liquid as:

$$\frac{1}{c_c^2} = \frac{\rho}{K} \tag{2.33}$$

The bulk modulus of a single bubble K_b is calculated from the radial displacement function as:

$$K_b(a_2, \omega) = \frac{a_2}{3} \frac{\hat{p}_i(\omega)}{\hat{\xi}(\omega)} \tag{2.34}$$

and the bulk modulus of the liquid is

$$K_L = \rho_L c_L \omega^2 \tag{2.35}$$

Density and bulk modulus of the bubbly liquid are calculated as the average of all components, integrating over all single MBs [16]. This leads to the speed of sound in bubbly liquid as follows:

$$\left(\frac{c_w}{c_c}\right) = 1 - 4\pi c_w \int_0^\infty \frac{a_2}{\omega_0} H\left(\frac{\omega}{\omega_0}\right) n(a_2) da_2 \tag{2.36}$$

The integral superposes all MBs, $n(a_2)da_2$ is the volume fraction of MBs in the suspension. eq. (2.28) and eq. (2.36) can now be combined to resolve for the complex number $u + jv$:

$$(u + jv)^2 = 1 - 4\pi c_w^2 \int_0^\infty \frac{a_2}{\omega_0} H(\frac{\omega}{\omega_0}) n(a_2) da_2 \tag{2.37}$$

Attenuation α and phase velocity c can be determined as

$$\alpha(\omega) = -20lg(e)\frac{\omega v}{c_w} = 20lg(e) \cdot Im\{k_c\} \tag{2.38}$$

$$c(\omega) = \frac{c_w}{u} = \frac{\omega}{Re\{k_c\}} \tag{2.39}$$

Attenuation of the MB suspension is thus related to k_i whereas phase velocity is closely related to k_r, as described in appendix A.2. Resolving of these eqautions for a monodisperse MB suspension with bubble diameter of $3\,\mu\mathrm{m}$ leads to the results produced by HOFF presented in fig. A.2 and fig. A.3.

Chapter 3

Experimental Methods

The characteristic curves for attenuation and phase velocity profile are acquired experimentally from the reflected time domain signal of an ultrasound pulse. In the following chapter both the experimental setup to gain the time domain signal and the data processing is described.

3.1 Experimental Setup

The experimental setup is similar to the setup described by KOTHAPALLI [17] and GRISHENKOV [12] and is presented in fig. 3.1.

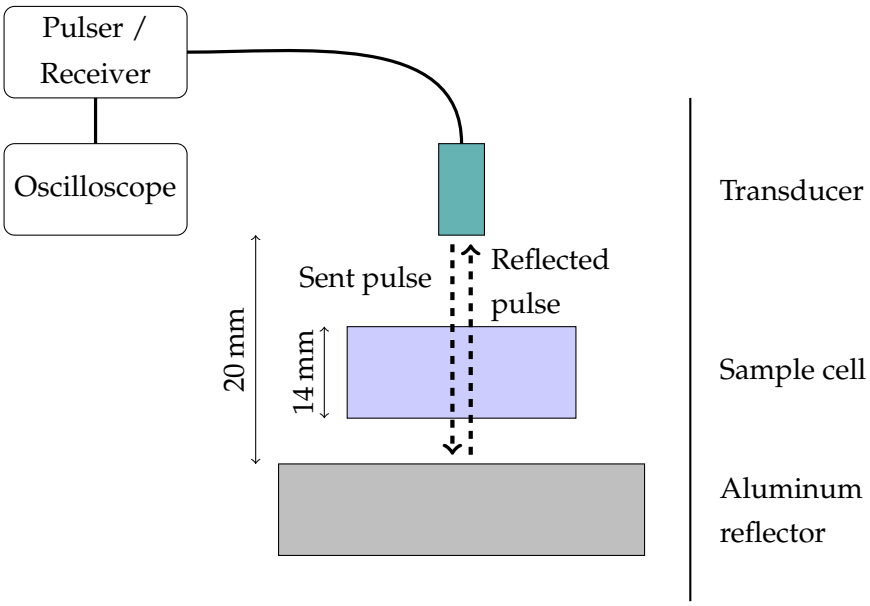

Figure 3.1: Experimental Setup

A flat transducers (Panametrics V311, Olympus NDT, Waltham, MA, USA)) is used for sending and detecting the ultrasound (US) pulse. The pulse is sent through the specimen and reflected at an aluminum plate back to the transducer. The distance between transducer and aluminum reflector is chosen smaller than near field length (NFL) of the US beam to 20 mm. The length of the specimen L is 14 mm. The sample cell contains two cells, one reference cell filled with water and one sample cell filled with MB suspension. The walls of the sample cell are thin compared to the wavelength of the transmitted signal. They act thus as acoustic window with a transmission coefficient $T = 1$ and effects from the walls on the reflected signal can be neglected. The specimen is excited by a gated pulse receiver in low power range (peak pressure $p_{i,max} < 100\,\mathrm{kPa}$).

3.1.1 Transducer range

Six narrow-band single crystal transducers with different center frequencies f_c are used to cover the frequency range between 1 and 15 MHz. The 6 dB band width (BW) is 50 % of the center frequency. However, the actual BW and peak frequency f_p differ from the values given in the data sheet. Peak frequencies, cut-off frequencies f_l and f_h as well as 6 dB BW are given in table 3.1.

Table 3.1: Transducer range for the 12 dB attenuation profile

$f_{c,expected}$ in MHz	$f_{c,actual}$ in MHz	f_p in MHz	f_l in MHz	f_h in MHz	BW in MHz
1	1.01	0.99	0.72	1.30	0.58
2.25	2.30	2.21	1.59	3.00	1.41
3.5	3.34	3.25	2.28	4.40	2.12
5	4.75	4.59	3.43	6.07	2.64
10	8.13	8.54	5.09	11.16	6.07
15	11.4	11.08	8.69	14.11	5.42

For the 3.5 to 15 MHz transducers the actual center frequency lies below the expected center frequency. This is due to the manufacturing process of the transducer. for For all transducers the pulse echo in both water and MB suspension is recorded.

3.1.2 Sensitivity of transducers

The signal measured by the transducers is most reliable at their peak frequency and only considered in the range between the cut-off frequencies f_l and f_h. The sensitivity of the transducer is considered as the power spectrum of the reference signal $P_{xx,ref}(\omega)$. The sensitivity curves for 12 dB profile are presented in fig. 3.2.

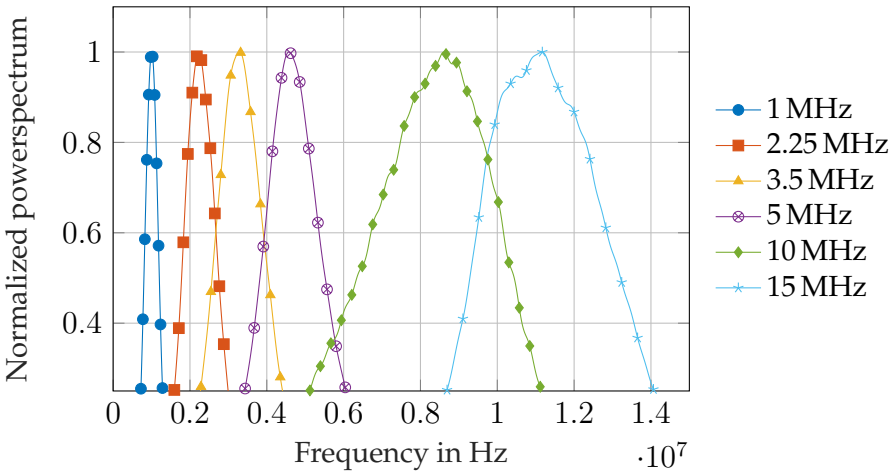

Figure 3.2: Sensitivity of the transducers, calculated for 12 dB profile

BWs of the single transducers is overlapping for all transducers

except a minor frequency range between 1 MHz and 2.25 MHz transducer. Thus a frequency range between 0.801 MHz and 13.22 MHz can be continuously covered by the measured data.

3.1.3 Microbubble suspension and particle size distribution

The experiment is carried out with polymer-shelled MBs as described in [10] and [18]. They contain a gas chore and a relatively thick rigid shell several hundreds of nm. Further information on the MB composition is given in appendix A.3.2.
The human body contains approximately 5 l blood. The volume of UCA introduced into the body is typically around 5 ml and usually has a concentration of $10^{12}\,\mathrm{l}^{-1}$ [24]. Diluted in the blood a concentration of $10^{9}\mathrm{l}^{-1}$ remains. The concentration of MBs in the sample cell is therefore chosen as $10^{9}\,\mathrm{l}^{-1}$. The size distribution of the bubbles is given as in fig. 3.3.

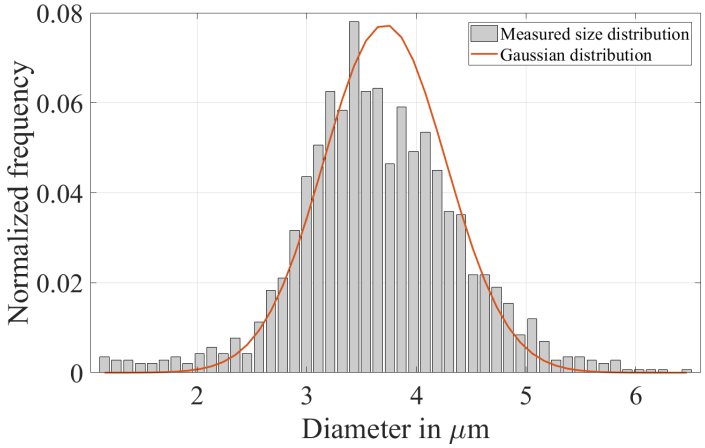

Figure 3.3: Measured size distribution of the MBs

However, the shell thickness is challenging to determine. Measurements have been done by KOTHAPALLI et al [17] claiming that the shell thickness is normal distributed with an average shell thickness of 315 nm.

3.2 Data processing

To reduce noise, averaging over 16 samples is used internally in the oscilloscope. The extracted signal is processed so that only the pulse echo is kept. To acquire attenuation and phase velocity curves the following steps are taken for each transducer:
The time domain signal received from water $s_{ref}(t)$ and from MB suspension $s_{MB}(t)$ are down-sampled to $2 \cdot f_h$ and a Hamming window is applied. The signal is then transformed into Frequency domain by usage of fast Fourier transform (FFT):

$$s_{ref}(t) \quad \circ\!\!-\!\!\bullet \quad \hat{s}_{ref}(\omega) = |\hat{s}_{ref}(\omega)| \cdot e^{j\varphi_{ref}(\omega)} \tag{3.1}$$

$$s_{MB}(t) \quad \circ\!\!-\!\!\bullet \quad \hat{s}_{MB}(\omega) = |\hat{s}_{MB}(\omega)| \cdot e^{j\varphi_{MB}(\omega)} \tag{3.2}$$

with $|\hat{s}(\omega)|$ being the magnitude of $\hat{s}(\omega)$ and $\varphi(\omega)$ being the phase. Harmonic decomposition of the signal is given by the back transformation from frequency to time domain introducing the complex wave number $k_c(\omega)$:

$$s(t) = \int_0^\infty \hat{s}(\omega, L) e^{j\omega t} d\omega = \int_{-\infty}^\infty \hat{s}_{ref}(\omega) e^{-jk_c(\omega)z} e^{j\omega t} d\omega \tag{3.3}$$

Attenuation and phase velocity curves are then determined from both signals in frequency domain following GRISHENKOV [12] and HOFF [14] as follows:

$$\alpha(\omega) = -\frac{20}{2L} \cdot log\left(\frac{|\hat{s}_{MB}(\omega, L)|}{|\hat{s}_{ref}(\omega)|}\right) \text{dB/unit length} \tag{3.4}$$

$$c(\omega) = \left[\frac{1}{c_{ref}} - \frac{\varphi_{MB} - \varphi_{ref}}{2L\omega}\right]^{-1} \text{m/s} \tag{3.5}$$

Note that phase velocity in water c_{ref} is not frequency dependent. More detailed descriptions can be found in appendix A.4.1 and appendix A.4.2.
However, whereas determining the magnitude of frequency domain signal and thus calculation of the attenuation profile is rather intuitive, some ambiguities can arise in the calculation of the phase.

3.2.1 Ambiguities in handling phase information

When calculating phase information very small numbers (in MATLAB called 'eps') may occur that can be amplified dramatically in further

signal processing, they should be masked out before calculating the phase difference.

A further issue is that after phase information being unwrapped there is still ambiguity in the phase difference of $2\pi n$ with n being an integer. As the phase velocity $c(\omega)$ is calculated relatively to the speed of sound in water c_w, the resulting $c(\omega)$ for each transducer crosses the value for c_w. To avoid this, an additional factor $2\pi n$ is introduced to the phase difference. n is chosen empirically so that the lowest mismatch and lowest dispersion occur. fig. 3.4 shows possible phase velocity curves depending on the value of n.

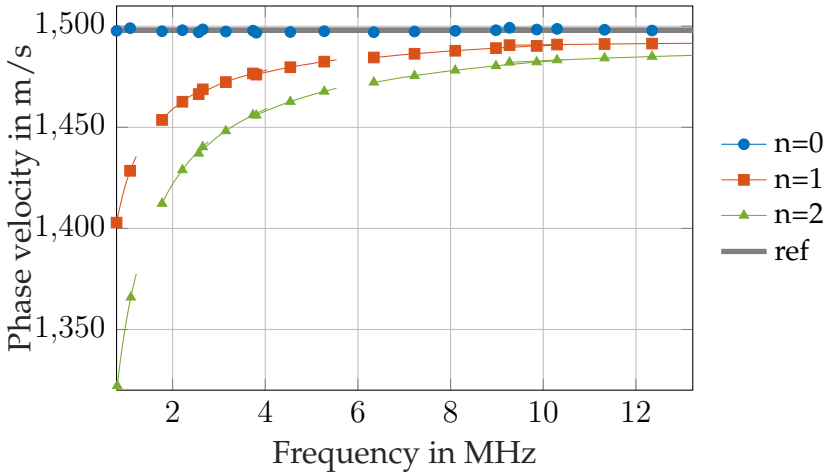

Figure 3.4: Change of phase velocity depending on phase difference of $2\pi n$

In lower frequency range the choice of n has significant influence on the phase velocity. To achieve the best match between the different transducers a value of $n = 1$ is chosen in further process.

Chapter 4

Post processing

In the following chapter the outcome of chapter 3 and chapter 2 is combined to reasonably predict shell parameters and resonance frequency of the MB suspension.

4.1 Measures for the goodness of fit

The Mean squared error (MSE) is a common measure to judge the quality of a fit and has been applied as single measure in former studies as done by FRINKING and DE JONG [7] or HOFF [13]. However, the MSE that considers absolute difference of two curves cannot account for structural similarities [19]. KOTHAPALLI et al [17] therefore introduced also the cross-correlation as measure of similarity between two curves. More detailed description of the effects is given in appendix B.

In the presented work both MSE and cross-correlation coefficient R are applied to compare model and experimental data. To account for reduced transducer sensitivity near cut-off frequencies the MSE was weighted using the sensitivity profile presented in fig. 3.2:

$$MSE_{weighted}(x, y) = \frac{1}{N} \sum_{i=1}^{N} (x_i - y_i)^2 \cdot P_{xx,ref,i} \tag{4.1}$$

where N is the length of the data set. As additional refinement criteria it is considered especially important that maximum of experimental and simulated data match. Therefore the frequency difference Δf_{max} is introduced as measure:

$$\Delta f_{max} = |f(x_{max}) - f(y_{max})| \tag{4.2}$$

This measurement is only done for attenuation curve since there is no specific feature to meet in the phase velocity curve.

4.2 Rank-based algorithm

In total five measures are taken: MSE, cross-correlation and frequency difference MSE_a, C_a and Δf for the attenuation curve, as well as MSE_p and C_p for the phase velocity curve, respectively. A rank-based algorithm as developed by SARANLI and DEMIREKLER [20] is used to combine the measures. Each of them is assigned a rank, rank one is assigned to the best solution according to the specific measure and the highest rank to the worst solution, respectively. Rank one is matched to the lowest MSE, cross-correlation closest to one and lowest frequency difference. The lowest value of summed up ranks gives the best compromise solution. An example is given in table 4.1.

Table 4.1: Extract of table to decide on the best parameter combination using SARANLI's and DEMIREKLER's rank-based algorithm

Solution	MSE_a	Rank	C_a	Rank	Δf_r	Rank	Sum
1	14.42	2	0.96	2	1.15 MHz	2	6
2	47.34	4	0.92	3	3.79 MHz	4	11
3	10.38	1	0.81	4	1.80 MHz	3	8
4	32.78	3	0.97	1	0.48 MHz	1	5

The table shows an extract from the simulation result, phase velocity curve measures are not considered in this example for reasons of space. In this specific case solution 4 yields the best compromise even if solution 3 has a lower MSE.

Chapter 5

Results

In the following chapter experimental results and results of the simulation are given.

5.1 Experimental

Following the procedure described in chapter 3 attenuation and phase velocity are determined experimentally for each transducer. The data is combined to cover the frequency range between 1 and 15 MHz. Attenuation and phase velocity coefficient are presented using the 12 dB transducer profile in fig. 5.1. Peak frequencies f_p of the transducers are marked to show the point of highest measurement accuracy. Attenuation is low in lower frequency range ($\approx 2.4\,\mathrm{dB/cm}$ at $f = 1\,\mathrm{MHz}$), but increases to a maximum at approximately $11 \text{ to } 12\,\mathrm{MHz}$. In high frequency range the attenuation decreases again. Underlying effects are described in appendix A.4.1. Phase velocity is significantly lower than in water in low frequency range ($\approx 1428\,\mathrm{m/s}$ at $f = 1\,\mathrm{MHz}$), but approaches the speed of sound in water at higher frequencies with approximately $1497\,\mathrm{m/s}$ at $f = 11\,\mathrm{MHz}$ compared to $1498\,\mathrm{m/s}$ in water.

5.2 Simulation

In the following the best parameter settings to model the MB oscillations are presented following the criteria described in chapter 4.

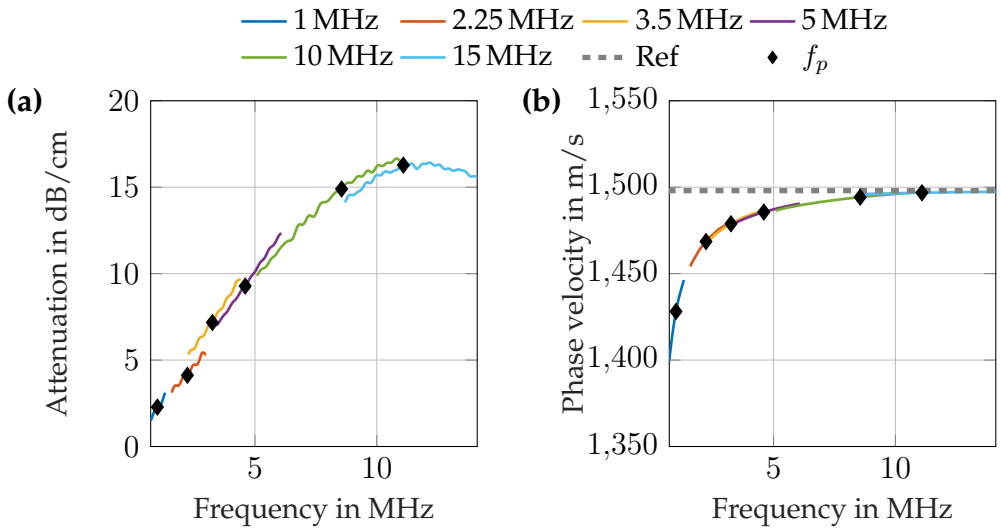

Figure 5.1: Experimentally acquired attenuation (a) and phase velocity coefficient (b) using the 12 dB transducer profile.

5.2.1 Simulation parameters

Constant parameters used for the simulation are listed in table 5.1.

Table 5.1: Constant simulation parameters

	Parameter	Value
General		
κ	Polytropic gas exponent	1
p_0	Atmospheric pressure	0.1 MPa
Liquid		
ρ_L	Liquid density	997 kg/m^3
η_L	Shear viscosity of liquid	$1 \cdot 10^{-3}$ Pa·s
c_L	Speed of sound in liquid	1498 m/s
Bubble		
ρ_S	Shell density	1053 kg/m^3

Parameters of the liquid ρ_L, η_L, c_L are given at a temperature of $T = 20\,^\circ\mathrm{C}$. The polytropic gas exponent is assumed to be 1 in an isothermal process. The variable parameters of the simulation are listed in table 5.2.

Table 5.2: Variable simulation parameters

	Parameter	Range
a_2	Initial outer bubble radius	1.62 to $2.89\,\mu\mathrm{m}$
d_s	Shell thickness	0.2 to $0.45\,\mu\mathrm{m}$
η_s	Shear viscosity of the shell	0.14 to $0.4\,\mathrm{Pa{\cdot}s}$
G_s	Shear modulus of the shell	8 to $20\,\mathrm{GPa}$

Bubble radius a_2 is acquired from experimental measurement of MB size distribution. Shell thickness d_s cannot be determined exactly under the microscope (compare POEHLMANN et al [21]). It is assumed to be either a certain percentage of a_2 or a constant value. POEHLMANN et al also showed that the shell thickness is approximately Gaussian distributed which will for simplicity reasons not be applied in the following, but delivers the range of d_s in the simulation. As the number of MBs in the suspension cannot be exactly controlled, but both attenuation and phase velocity magnitude react sensitively to changes in concentration, small variations of max. 10 % are accepted in the model.

5.2.2 Simulation results

Exact shell thickness distribution is unknown, therefore two possible distributions are assumed leading to different results. Shell thickness can be assumed to be either constant for all MBs independently of outer radius or considered to be a fixed percentage of the outer radius.

Constant shell thickness

Good agreement was achieved for the following parameters: shear modulus $G_s = 16.5\,\mathrm{MPa}$, shear viscosity $\eta_s = 0.325\,\mathrm{Pa{\cdot}s}$ and shell thickness $d_s = 360\,\mathrm{nm}$. In that case $C_a \approx C_p \approx 1$, the values of all measures can be seen in table 5.3.

Table 5.3: Measures for the goodness-of-fit assuming a constant shell thickness

	MSE	C	Δf_r in MHz
Attenuation	1.46	0.9952	0.564
Phase Velocity	43.21	0.9466	-

Resonance frequency of the suspension is calculated as 11.6 MHz. The damping ratio for the mean outer bubble radius is shown in fig. 5.2. Using the parameters presented above leading to the presented res-

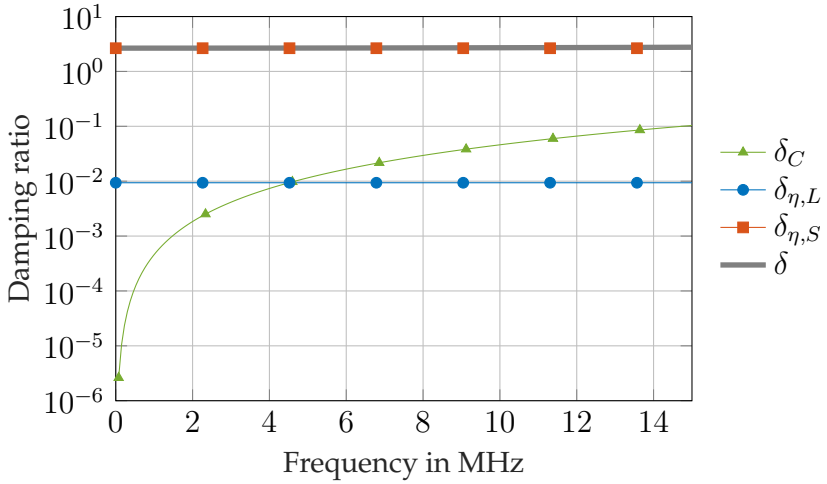

Figure 5.2: Frequency dependent damping ratio for the mean outer bubble radius and assuming constant shell thickness

onance frequency and damping ratio, the resulting attenuation and phase velocity curves are shown in fig. 5.3. The dashed line shows experimental data, the solid line theoretically modeled data. Both attenuation and phase velocity curve are very closely met in frequency range around resonance. However, in lower frequency range the experimentally acquired curve differs from the modeled curve, especially in the phase velocity coefficient.

Shell thickness relative to outer shell radius

Shell thickness between 15 % and 30 % of the outer bubble radius is examined, best results were achieved for the following parameters: $G_s = 14.5\,\mathrm{MPa}$, $\eta_s = 0.322\,\mathrm{Pa{\cdot}s}$, $d_s = 0.16 \cdot a_2$. The measures for this fit are presented in table 5.4.

Table 5.4: Measures for the goodness-of-fit

	MSE	C	Δf_r in MHz
Attenuation	0.89	0.9955	0.489
Phase Velocity	41.80	0.9576	-

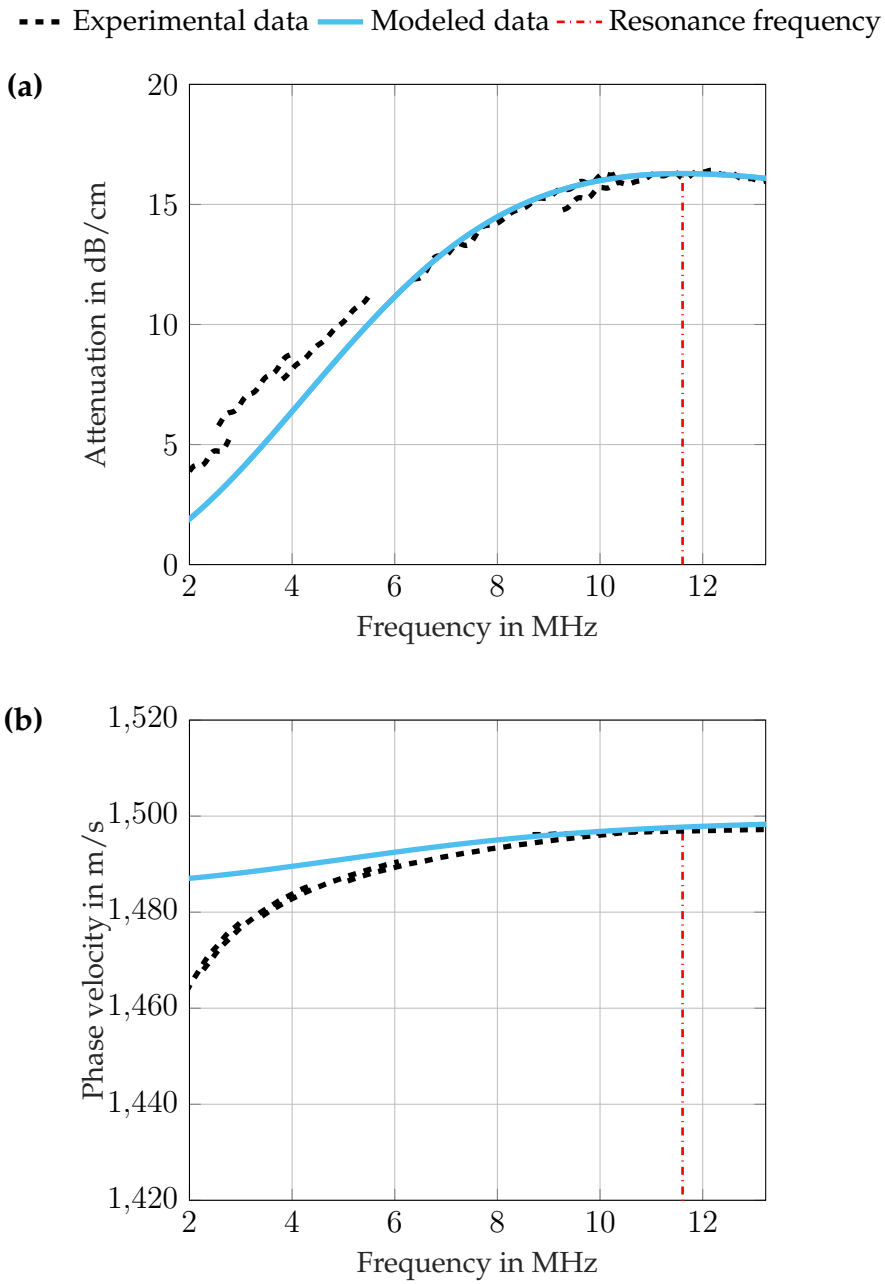

Figure 5.3: Assumption: shell thickness is a constant. Experimentally measured and theoretically modeled attenuation **(a)** and phase velocity **(b)** profiles.

All measures are slightly better than for the solution assuming constant shell radius. Resonance frequency is calculated to $f_r = 11.68\,MHz$

which is comparable to the previous solution. The damping coefficients for this solution are presented in fig. 5.4.

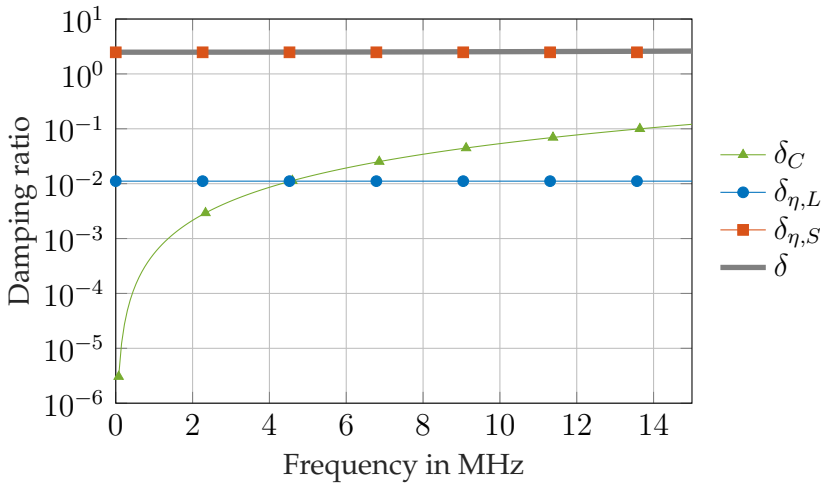

Figure 5.4: Frequency dependent damping ratio for the mean outer bubble radius and assuming $d_s \propto a_2$

The resulting distribution of the shell thickness is presented in fig. 5.5, which is based on the size distribution given in fig. 3.3.

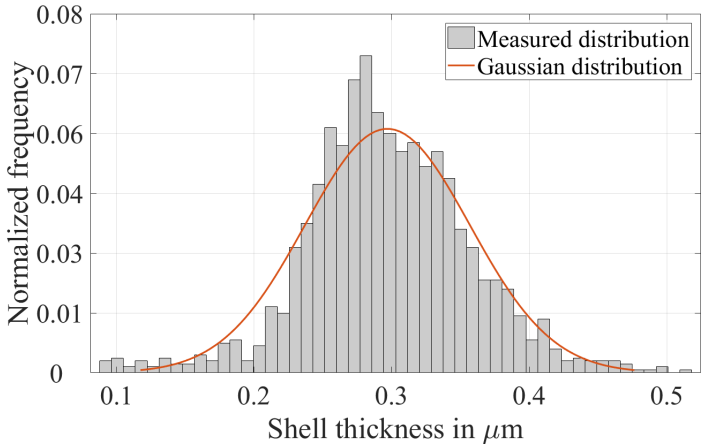

Figure 5.5: Distribution of the shell thickness, when it is assumed to be 16 % of the outer bubble radius

Determined from the size distribution the most frequent value of shell thickness is 275 nm. Attenuation and phase velocity coefficients

are presented in fig. 5.6. The solution contains similar effects as the

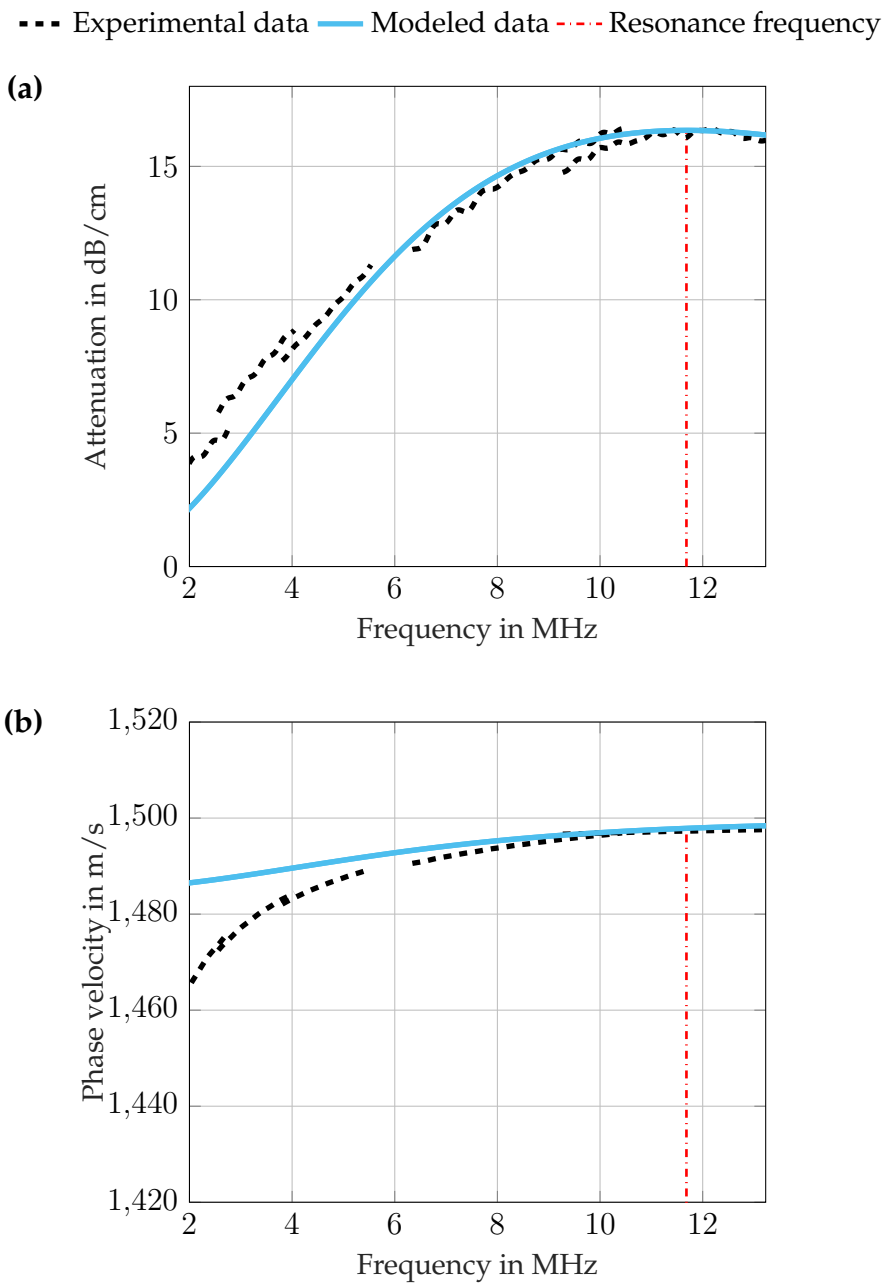

Figure 5.6: Assumption: shell thickness is relative to outer bubble radius. Experimentally measured and theoretically modeled attenuation **(a)** and phase velocity **(b)** profiles.

constant shell thickness solution. Around resonance frequency both

experimental attenuation and phase velocity coefficient are closely met in the model where accordance decreases at lower frequency range. Final output parameters of both approaches are presented in table 5.5.

Table 5.5: Output parameters of both approaches constant d_s and d_s proportional to outer shell radius

	G_s	η_s	d_s	f_r
$d_s\ const.$	16.5 MPa	0.325 Pa·s	360 nm	11.61 MHz
$d_s \propto a_2$	14.5 MPa	0.322 Pa·s	$0.16 \cdot a_2$	11.68 MHz

Chapter 6

Discussion

In the presented work frequency dependent attenuation and phase velocity coefficients in a suspension of PVA shelled MBs with concentration of $10^6\,\mathrm{ml}^{-1}$ were measured and modeled. The model was fitted to the experimental data.

Measures for goodness of fit

For calculating the goodness of fit both MSE and cross-correlation for both attenuation and phase velocity were used as well as the difference between experimental and modeled maximum attenuation. MSE as well established standard measure accounts for the absolute error of the modeled data and is uncritical to use as measure for goodness of fit. The cross-correlation is mainly used in signal processing and allows a judgment for the similarity of the shape of two curves. This measure is sensitive to use. For the attenuation coefficient using the parameters given in table 5.2, 77 % of the simulated curves lead to a cross-correlation $C > 0.99$. Comparison in this measure acts thus in a very small range of less than 0.1 % of the measurement scale. For laying extra focus on the accordance between the maximums of modeled and measured attenuation curve, the difference between both was minimized. This improves the overall fitting results significantly. However, experimental data includes some noise which makes its maximum not an ideal reference.

Rank-based algorithm

To consider all measures for the goodness of fit a rank-based algorithm is used. This has been applied in some similar studies before (see [17]). Every measure is weighted equally meaning all measures get equal influence in the final plot, which is both the advantage and a draw-back of the algorithm. Inclusion of different measures is easily possible by this method, but less relevant measures may get overweighted. In the presented study measures were not weighted since no profound sign was found to justify a weighing of the measures in a certain manner.

Experimental Results

Attenuation curves are calculated from the FFT's magnitude and unambiguous to determine. Phase velocity curves are calculated from the phase of the FFT which is periodic with 2π. Therefore, phase velocity cannot be calculated unambiguous leaving room for unexpected behaviour as non-spherical oscillations in the low-frequency range. In the presented work n was chosen empirically for lowest mismatch between the different transducer curves and lowest dispersion. To further examine phase velocity in detail, other methods to calculated the phase such as phase locking need to be considered.

Shell thickness

An uncertain parameter in the model is the shell thickness of the bubbles. Assumptions of both constant shell thickness and thickness proportional to the outer bubble radius have been made. Measurements were performed leading to a range of possibilities including shell thickness range of $0.2 to 0.45\,\mu\mathrm{m}$ [21] or 10 to $40\,\%$ of the external radius [12]. In the presented work both assumptions were modeled and fitted to the experimental data leading to similar results in term of measures for goodness of fit and similar resonance frequency. The shell parameters differ part-wise, but are in the same order of magnitude. Still it cannot be assured that the correct shell thickness distribution is met in the presented work and remains the most critical parameter in the model.

Simulation results

In both approaches to model shell thickness attenuation and phase velocity curves are closely met around resonance of the bubble suspension, but differ from the experimental data in lower frequency range. This might be due to non-exact assumptions concerning shell thicknesses, since shell thickness is a sensitive parameter in the model. Other reasons might be additional damping at lower frequencies which was not considered in the presented model. Furthermore, both shear viscosity and shear modulus could be assumed to be a frequency dependent parameter to improve the fitting quality.

Chapter 7

Conclusion and Future Work

In the presented work a procedure was designed to characterize UCAs non-destructively.
Therefore, the MB was modeled combining the models of HOFF and CHURCH. The components of a linear oscillator modeling a single bubble was adjusted to be suitable for bubbles of any shell thickness. Superposing the behaviour of all MBs in the suspension attenuation and phase velocity profile were extracted.
The echo signal of a short US pulse sent through the suspension at different center frequencies was measured in time domain and processed to experimentally determine attenuation and phase velocity coefficients. Compared to former studies higher measurement accuracy was achieved over a broader frequency range through combination of different narrow-band single crystal ultrasound transducers.
Viscoelastic parameters of the shell were estimated as well as the resonance frequency of the bubble suspension by fitting the model to the experimental data. This was done considering MSE and cross-correlation for both attenuation and phase velocity curve, also comparison of the curve maxima in the attenuation curve.
Parameter setting were optimized and the model could be well matched to the experimental data. Still some mismatches remain especially in lower frequency range. Very good matches could be achieved around the resonance frequency which for the given MB suspension lays at $f_r \approx 11.6\,\mathrm{MHz}$.
As discussed in chapter 6 in the future some refinements need to be done in the shell thickness assumption. The model may be adjusted to achieve a better match in lower frequency range. In experimental data

acquisition improvements may be made to avoid ambiguities in phase velocity calculation. Methods that should be investigated are Hilbert transform and phase locking instead of FFT.
The outcome of this thesis can then be used to characterize different kinds of air or gas MB suspensions and compare them. If all parameters are known the model can be used to predict resonance frequency in suspensions of different concentration or surrounding liquid.

Bibliography

[1] P. R. Hoskins, K. Martin, and A. Thrush, *Diagnostic ultrasound: physics and equipment*. Cambridge University Press, 2010.

[2] N. de Jong, L. Hoff, T. Skotland, and N. Bom, "Absorption and scatter of encapsulated gas filled microspheres: Theoretical considerations and some measurements", *Ultrasonics*, vol. 30, no. 2, pp. 95–103, 1992.

[3] F. Cavalieri, A. El Hamassi, E. Chiessi, and G. Paradossi, "Stable polymeric microballoons as multifunctional device for biomedical uses: Synthesis and characterization", *Langmuir*, vol. 21, no. 19, pp. 8758–8764, 2005.

[4] B. Cerroni, E. Chiessi, S. Margheritelli, L. Oddo, and G. Paradossi, "Polymer shelled microparticles for a targeted doxorubicin delivery in cancer therapy", *Biomacromolecules*, vol. 12, no. 3, pp. 593–601, 2011.

[5] K. Kooiman, H. J. Vos, M. Versluis, and N. de Jong, "Acoustic behavior of microbubbles and implications for drug delivery", *Advanced drug delivery reviews*, vol. 72, pp. 28–48, 2014.

[6] M. S. Plesset, "The dynamics of cavitation bubbles", *Journal of applied mechanics*, vol. 16, pp. 277–282, 1949.

[7] P. J. Frinking and N. de Jong, "Acoustic modeling of shell-encapsulated gas bubbles", *Ultrasound in medicine & biology*, vol. 24, no. 4, pp. 523–533, 1998.

[8] P. Marmottant, S. van der Meer, M. Emmer, M. Versluis, N. de Jong, S. Hilgenfeldt, and D. Lohse, "A model for large amplitude oscillations of coated bubbles accounting for buckling and rupture", *The Journal of the Acoustical Society of America*, vol. 118, no. 6, pp. 3499–3505, 2005.

[9] K. Sarkar, W. T. Shi, D. Chatterjee, and F. Forsberg, "Characterization of ultrasound contrast microbubbles using in vitro experiments and viscous and viscoelastic interface models for encapsulation", *The Journal of the Acoustical Society of America*, vol. 118, no. 1, pp. 539–550, 2005.

[10] M. Tortora, L. Oddo, S. Margheritelli, and G. Paradossi, "Design of novel polymer shelled ultrasound contrast agents: Towards an ultrasound triggered drug delivery", in *Ultrasound Contrast Agents*, Springer, 2010, pp. 25–39.

[11] C. C. Church, "The effects of an elastic solid surface layer on the radial pulsations of gas bubbles", *The Journal of the Acoustical Society of America*, vol. 97, no. 3, pp. 1510–1521, 1995.

[12] D. Grishenkov, C. Pecorari, T. B. Brismar, and G. Paradossi, "Characterization of acoustic properties of pva-shelled ultrasound contrast agents: Linear properties (part i)", *Ultrasound in medicine & biology*, vol. 35, no. 7, pp. 1127–1138, 2009.

[13] L. Hoff, P. C. Sontum, and J. M. Hovem, "Oscillations of polymeric microbubbles: Effect of the encapsulating shell", *The Journal of the Acoustical Society of America*, vol. 107, no. 4, pp. 2272–2280, 2000.

[14] L. Hoff, *Acoustic characterization of contrast agents for medical ultrasound imaging*. Springer Science & Business Media, 2001.

[15] K. W. Commander and A. Prosperetti, "Linear pressure waves in bubbly liquids: Comparison between theory and experiments", *The Journal of the Acoustical Society of America*, vol. 85, no. 2, pp. 732–746, 1989.

[16] T. Leighton, *The acoustic bubble*. Academic press, 2012.

[17] S. V. Kothapalli, L. Oddo, G. Paradossi, L.-Å. Brodin, and D. Grishenkov, "Assessment of the viscoelastic and oscillation properties of a nano-engineered multimodality contrast agent", *Ultrasound in medicine & biology*, vol. 40, no. 10, pp. 2476–2487, 2014.

[18] M. Zheng, *Ultrasound contrast agents: Fabrication, size distribution and visualization*, 2011.

[19] Z. Wang and A. C. Bovik, "Mean squared error: Love it or leave it? a new look at signal fidelity measures", *IEEE signal processing magazine*, vol. 26, no. 1, pp. 98–117, 2009.

[20] A. Saranli and M. Demirekler, "A statistical unified framework for rank-based multiple classifier decision combination", *Pattern Recognition*, vol. 34, no. 4, pp. 865–884, 2001.

[21] M. Poehlmann, D. Grishenkov, S. V. Kothapalli, J. Härmark, H. Hebert, A. Philipp, R. Hoeller, M. Seuss, C. Kuttner, S. Margheritelli, *et al.*, "On the interplay of shell structure with low-and high-frequency mechanics of multifunctional magnetic microbubbles", *Soft Matter*, vol. 10, no. 1, pp. 214–226, 2014.

[22] J.-M. Correas, L. Bridal, A. Lesavre, A. Méjean, M. Claudon, and O. Hélénon, "Ultrasound contrast agents: Properties, principles of action, tolerance, and artifacts", *European radiology*, vol. 11, no. 8, pp. 1316–1328, 2001.

[23] S. M. van der Meer, B. Dollet, M. M. Voormolen, C. T. Chin, A. Bouakaz, N. de Jong, M. Versluis, and D. Lohse, "Microbubble spectroscopy of ultrasound contrast agents", *The Journal of the Acoustical Society of America*, vol. 121, no. 1, pp. 648–656, 2007.

[24] H. Becher and P. N. Burns, *Handbook of contrast echocardiography: Left ventricular function and myocardial perfusion*. Springer Science & Business Media, 2012.

[25] P. Krishna, P. Shankar, and V. Newhouse, "Subharmonic generation from ultrasonic contrast agents", *Physics in Medicine & Biology*, vol. 44, no. 3, p. 681, 1999.

[26] N. de Jong, M. Emmer, A. Van Wamel, and M. Versluis, "Ultrasonic characterization of ultrasound contrast agents", *Medical & biological engineering & computing*, vol. 47, no. 8, pp. 861–873, 2009.

[27] M. Emmer, H. J. Vos, D. E. Goertz, A. van Wamel, M. Versluis, and N. de Jong, "Pressure-dependent attenuation and scattering of phospholipid-coated microbubbles at low acoustic pressures", *Ultrasound in medicine & biology*, vol. 35, no. 1, pp. 102–111, 2009.

[28] A. Kabalnov, D. Klein, T. Pelura, E. Schutt, and J. Weers, "Dissolution of multicomponent microbubbles in the bloodstream: 1. theory", *Ultrasound in medicine & biology*, vol. 24, no. 5, pp. 739–749, 1998.

[29] J.-M. Correas and O. c. Helenon, "Ultrasound contrast agents. examples of blood pool agents.", *Acta radiologica. Supplementum*, vol. 412, pp. 101–112, 1997.

[30] T. Faez, M. Emmer, K. Kooiman, M. Versluis, A. F. van der Steen, and N. de Jong, "20 years of ultrasound contrast agent modeling", *IEEE transactions on ultrasonics, ferroelectrics, and frequency control*, vol. 60, no. 1, 2013.

[31] K. Kooiman, M. R. Böhmer, M. Emmer, H. J. Vos, C. Chlon, W. T. Shi, C. S. Hall, S. H. de Winter, K. Schroën, M. Versluis, *et al.*, "Oil-filled polymer microcapsules for ultrasound-mediated delivery of lipophilic drugs", *Journal of controlled release*, vol. 133, no. 2, pp. 109–118, 2009.

[32] K. K. Shung, *Diagnostic Ultrasound*. CRC Press, 2006.

[33] B. Zhao, O. Basir, and G. Mittal, "Estimation of ultrasound attenuation and dispersion using short time fourier transform", *Ultrasonics*, vol. 43, no. 5, pp. 375–381, 2005.

[34] P. He, "Direct measurement of ultrasonic dispersion using a broadband transmission technique", *Ultrasonics*, vol. 37, no. 1, pp. 67–70, 1999.

[35] C. K. Holland, C. X. Deng, R. E. Apfel, J. L. Alderman, L. A. Fernandez, and K. J. Taylor, "Direct evidence of cavitation in vivo from diagnostic ultrasound", *Ultrasound in Medicine and Biology*, vol. 22, no. 7, pp. 917–925, 1996.

[36] P. He, "Simulation of ultrasound pulse propagation in lossy media obeying a frequency power law", *ieee transactions on ultrasonics, ferroelectrics, and frequency control*, vol. 45, no. 1, pp. 114–125, 1998.

[37] N. de Jong, A. Bouakaz, and P. Frinking, "Basic acoustic properties of microbubbles", *Echocardiography*, vol. 19, no. 3, pp. 229–240, 2002.

[38] M. Overvelde, H. J. Vos, N. de Jong, and M. Versluis, "Ultrasound contrast agent microbubble dynamics", in *Ultrasound Contrast Agents*, Springer, 2010, pp. 79–97.

[39] C. E. Brennen, *Cavitation and bubble dynamics*. Cambridge University Press, 2013.

[40] V. Bjerknes, *Fields of force*. General Books, 1906.

[41] P. A. Dayton, J. S. Allen, and K. W. Ferrara, "The magnitude of radiation force on ultrasound contrast agents", *The Journal of the Acoustical Society of America*, vol. 112, no. 5, pp. 2183–2192, 2002.

[42] H. J. Vos, B. Dollet, J. Bosch, M. Versluis, and N. De Jong, "Nonspherical vibrations of microbubbles in contact with a wall—a pilot study at low mechanical index", *Ultrasound in medicine & biology*, vol. 34, no. 4, pp. 685–688, 2008.

[43] V. Garbin, D. Cojoc, E. Ferrari, E. Di Fabrizio, M. Overvelde, S. Van Der Meer, N. De Jong, D. Lohse, and M. Versluis, "Changes in microbubble dynamics near a boundary revealed by combined optical micromanipulation and high-speed imaging", *Applied physics letters*, vol. 90, no. 11, p. 114 103, 2007.

[44] J.-M. Gorce, M. Arditi, and M. Schneider, "Influence of bubble size distribution on the echogenicity of ultrasound contrast agents: A study of sonovue™", *Investigative radiology*, vol. 35, no. 11, pp. 661–671, 2000.

[45] N. de Jong, P. J. Frinking, A. Bouakaz, M. Goorden, T. Schourmans, X. Jingping, and F. Mastik, "Optical imaging of contrast agent microbubbles in an ultrasound field with a 100-mhz camera", *Ultrasound in medicine & biology*, vol. 26, no. 3, pp. 487–492, 2000.

[46] D. Grishenkov, "Polymer-shelled ultrasound contrast agents: Characterization and application", PhD thesis, KTH, 2010.

[47] L. Rayleigh, "On the pressure developed in a liquid during the collapse of a spherical cavity", *The London, Edinburgh, and Dublin Philosophical Magazine and Journal of Science*, vol. 34, no. 200, pp. 94–98, 1917.

[48] M. Minnaert, "On musical air-bubbles and the sounds of running water", *The London, Edinburgh, and Dublin Philosophical Magazine and Journal of Science*, vol. 16, no. 104, pp. 235–248, 1933.

[49] N. de Jong, R. Cornet, and C. d. Lancée, "Higher harmonics of vibrating gas-filled microspheres. part one: Simulations", *Ultrasonics*, vol. 32, no. 6, pp. 447–453, 1994.

[50] A. A. Doinikov, J. F. Haac, and P. A. Dayton, "Resonance frequencies of lipid-shelled microbubbles in the regime of nonlinear oscillations", *Ultrasonics*, vol. 49, no. 2, pp. 263–268, 2009.

[51] J. McLaughlan, N. Ingram, P. R. Smith, S. Harput, P. L. Coletta, S. Evans, and S. Freear, "Increasing the sonoporation efficiency of targeted polydisperse microbubble populations using chirp excitation", *IEEE transactions on ultrasonics, ferroelectrics, and frequency control*, vol. 60, no. 12, pp. 2511–2520, 2013.

[52] P. Marmottant, M. Versluis, N. de Jong, S. Hilgenfeldt, and D. Lohse, "High-speed imaging of an ultrasound-driven bubble in contact with a wall:"narcissus" effect and resolved acoustic streaming", *Experiments in fluids*, vol. 41, no. 2, pp. 147–153, 2006.

[53] H. J. Vos, B. Dollet, M. Versluis, and N. De Jong, "Nonspherical shape oscillations of coated microbubbles in contact with a wall", *Ultrasound in medicine & biology*, vol. 37, no. 6, pp. 935–948, 2011.

[54] S. Zhao, K. W. Ferrara, and P. A. Dayton, "Asymmetric oscillation of adherent targeted ultrasound contrast agents", *Applied physics letters*, vol. 87, no. 13, p. 134 103, 2005.

Appendix A

Literature Review

In the following chapter the state of the art in UCA characterization is described. This is a summary of earlier publications and does not describe the author's own work.

A.1 The use of ultrasound contrast agents

An UCA is defined as exogenous substance that can be administered, either in the blood pool or in a cavity, to enhance the ultrasound signal [22]. Ultrasound scatter from blood is usually much weaker than scatter from tissue [23] and therefore blood vessels are difficult to image in ultrasound. UCAs can increase the backscattered signal intensity dramatically and therefore enhance the contrast of the image when injected into blood vessels.
To be both useful and safe in clinical use, an UCA needs to be easily introducible into the vascular system, be stable during the examination, have low toxicity and modify at least one acoustic property as acoustic attenuation (see appendix A.2) of the tissue [24].

A.1.1 Microbubbles as ultrasound contrast agent

Mostly microbubbles (MBs) are used as UCA which are excellent ultrasound scatterers because of the impedance mismatch between liquid and gas chore [25]. That is, a bubble is about one hundred million times more effective at scattering ultrasound than tissue [24]. Furthermore MBs are smaller than red blood cells and can thus pass capillaries circulate nearly freely in the blood flow. An average UCA contains

billions of MB per ml that act as a resonant system: they increase the energy in the backscattered signal at the initial frequency with the displacement being maximum at resonance frequency, but also transferring energy to subharmonics and ultra-harmonics [26]. The latter is useful in ultra-harmonic imaging, since tissue scatters mostly linearly and by filtering out the incident frequency from the received signal, the contrast enhancement due to UCA can be even amplified [27].

A.1.2 Composition of microbubbles

A perfect blood pool agent displays the same flow dynamics as the blood itself and is ultimately metabolized from the blood flow [24]. The most intuitive approach to this is the use of free air bubbles. Their theoretical behaviour is described in appendix A.5. Due to the limited persistence and efficacy free air bubbles are rarely used in medical applications, instead nowadays mostly galactose or albumin are in use [22]. In research or pre-clinical PVA shelled MBs are of actual interest. They usually contain bubbles of a polydisperse size distribution with diameters between 1 and $10\,\mu\mathrm{m}$ and a mean diameter of 2 to $3\,\mu\mathrm{m}$ [26]. The size distribution is difficult to measure since it depends on the environment of the bubble as surface tension at the gas-liquid interface, hydrostatic and acoustic pressure. The aim is to achieve a Gaussian distribution that is as narrow as possible.
The Ostwald coefficient describes the ratio of the solubility of a gas in liquid to gas density and is thus a parameter dissolution of bubbles [28]. Air-filled bubbles usually have a dissolution speed of 40 to 50 ms which can be greatly extended by the use of low-solubility gases that slower the process of diffusion. These heavy molecular weight inert gases such as $\mathrm{SF_6}$, $\mathrm{C_3F_8}$, $\mathrm{C_4F_{10}}$ increase the Ostwald coefficient, but at the same time reduce the acoustic responsiveness of the agent [29].
Encapsulation of the MB offers the advantages of increased lifespan, the ability to pass the lungs and reduction of the surface tension [30]. One usually differentiates between flexible coatings of phospholipids (shell thickness of a few nm) and solid encapsulation using f.ex. polymers (shell thickness of tens to hundreds of nm).

Polymer shelled microbubbles

There are several limitations in the use of lipid shelled (flexible coated) as targeted MBs. Due to their high dimensional variability and short

circulation time and low stability in the blood stream, the field of drugs that can be attached to the bubbles is restricted. Instead bubbles coated by synthetic polymer with good biocompatibility properties can be used. The MBs used in the presented work consist of a shell of loosely arranged PVA fibrils. In the inner region the polymeric material is more compact whereas the outer cross-linked PVA chains are extending into solution. [10]
Polymer coatings are very rigid and increase resonance frequency of the bubbles to $> 15\,\mathrm{MHz}$ for capsules of $3\,\mu\mathrm{m}$ [31]. Determination of the resonance frequency is described in appendix A.6.

A.2 Physical properties of the ultrasound beam

As a sound wave passes through medium it causes the particles to oscillate along the line of wave propagation. By that a harmonic pressure change is introduced into the medium. The difference between this actual pressure and normal rest pressure in the medium is called excess pressure and measured in pascal. [1]
The propagation of a plane harmonic wave is described by a complex wave number k_c:

$$p(z,t) = p_0 \cdot e^{j(\omega t - k_c z)} = p_0 \cdot e^{k_i z} \cdot e^{j(\omega t - k_r z)} \tag{A.1}$$

with $p(z,t)$ being the acoustic pressure, p_0 being ambient pressure and

$$k_c = k_r + jk_i \tag{A.2}$$

being the complex wave number [14]. z is distance, t time and w the angular frequency of the traveling wave. As can be seen from the equation the amplitude of p is dependent on k_i whereas the phase depends on k_r. This introduces the concept of attenuation and phase velocity described below.

- **Attenuation** describes the energy of the ultrasound wave that is lost over traveled distance [1]. Enhancement of attenuation increases the visibility of desired tissue, but decreases the contrast distal to the enhanced region [32].
- **Phase velocity** is defined as the propagation velocity of a sinusoidal wave at a given frequency in the medium [33].

- **Dispersion** is determined as the change in phase velocity in a medium [34].

When ultrasound propagates through a medium as tissue or a given specimen the beam is reflected and transmitted at the boundaries between different media. Both effects are dependent on the acoustic impedance match of the two media at the boundary. The transmission coefficient names the percentage of the incident wave amplitude that is transmitted to the next material whereas the reflection coefficient describes the percentage of the incident wave amplitude reclected at a boundary. Reflection occurs at large interfaces as between different organs. In case the second media is very small as the later introduced MBs reflection does not follow the law of reflection but scatters the waves in different angles.. [1]

The ultrasound image is formed by both reflected and scattered ultrasound beams.

Describing the effect on tissue

Applying an ultrasound beam to tissues has both a thermal and a mechanical (cavitational) effect. The latter is characterized by the mechanical index (MI) defined by APFEL [35] as

$$MI = \frac{P_{np}}{\sqrt{f_c}} \tag{A.3}$$

with P_{np} being the peak negative pressure and f_c being the center frequency of the ultrasound wave. MI is regarded as dimensionless number [5] and is related to the amount of mechanical work that can be performed on a bubble during a single negative half cycle of sound. The higher the MI the more likely it is that cavitation effects occur. In practice the MI varies among the image, but nevertheless it is one of the most important parameters in a contrast image study. [24]

A.3 Acoustic behaviour of microbubbles in the ultrasonic field

When an ultrasound wave passes through a medium the waveform of the original ultrasound signal is changed as a result of both dispersion and attenuation (see appendix A.2), [36]). The bubbles within

the suspension will react with volume pulsations, either linearly or non-linearly and eventually crack [26]. As the acoustic pressure increases, the MB will compress, at falling pressure amplitude it extends. Compression and extension of the bubble at low acoustic pressures is schematically shown in fig. A.1.

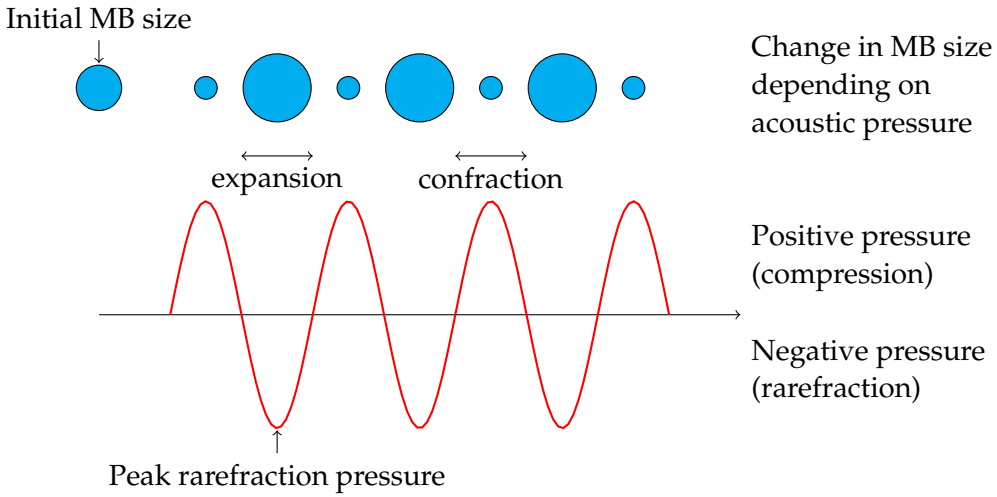

Figure A.1: Schematic diagram showing microbubble oscillations at low acoustic pressures [1]

PVA shelled MBs provide a bulk modulus of $2.5\,\mathrm{MPa}$ compared to air that has a bulk modulus of $0.1\,\mathrm{MPa}$ [14]. That makes MBs suitable as ultrasound scatterers. Depending on shell and excitation signal the bubble can compress by over 50 % of the initial radius and expand by several factors of the initial radius [37]. The MB in the ultrasonic field will thus act as a resonant system backscattering harmonic energy. However, the type and characteristics of the oscillation are a complex interaction and dependent on signal properties, agent properties and bubble position. At low concentrations $(10^{-5}$ to $10^{-6})$ bubble oscillations do not interact [14]. This will be described briefly in the following.

A.3.1 Dependence on signal properties and the linear regime

The MB suspension behaves differently depending on signal power and frequency. At lower excitation powers ($MI < 0.1$, $p_i < 100\,\mathrm{kPa}$) the reflected signal shows a very weak non-linear response of both MB and tissue and can thus regarded as linear. The amount of scattering and attenuation of the signal is also dependent on the frequency of the incident wave. The damping and thus attenuation is highest at resonance frequency (see appendix A.6) and usually lies in the range of 10 to 20 % of the incident amplitude for an oscillating gas bubble in micrometer size at resonance [37]. Resonance occurs for a $4\,\mu\mathrm{m}$ free gas bubble at ca $1.6\,\mathrm{MHz}$ [26]. Through coating both the damping coefficient and resonance frequency can be increased, for ex. elastic coating of phospholipids increases resonance frequency with up to 40 % [23]. As the acoustic power is increased above $100\,\mathrm{kPa}$ non-linear effects increase and become more relevant. Backscattered energy at higher harmonics and subharmonics is produced [38]. Since the presented work focuses on characterization in the linear regime no further explanations concerning high-pressure behaviour will be given.

A.3.2 Dependence on bubble and shell properties

Bubble behaviour is strongly influenced by the bubble properties, mainly bubble radius and shell parameters such as stiffness and thickness. The scattering efficiency is proportional to a_2^6 with a_2 being the bubble radius, so the larger te bubble the higher the scattering efficiency [22]. At the same time it is not possible to make infinitely large bubbles since they need to float freely in the blood pool. Most MBs have a radius between $2\,\mu\mathrm{m}$ and $10\,\mu\mathrm{m}$. An uncoated bubble may survive for 80 ms when acoustically excited with continuous waves [16]. Adding a shell with a certain shell stiffness and using high-molecular-weight gases as filling decreases the backscattered response but dramatically increases stability of the bubble [22]. The acoustic behaviour is significantly changed through encapsulation. Higher shell stiffness increases the resonance frequency of the bubble whereas higher viscosity of the shell increases the damping [26]. A thicker shell also increases the resonance frequency.

A.3.3 Radiation force

In a propagating wave an oscillating MB can translate through radiation force in the direction of the traveling wave [39], [16]. The translation speed of the MBs is comparable to the speed of regular blood flow [5]. According to BJERKNES et al [40] two different radiation forces exist: primary Bjerknes force is the radiation force resulting on the incident wave whereas secondary Bjerknes force is excited from a nearby bubble that is within the same field. This causes different effects: MBs will be pushed to the distal wall in a medical ultrasound field due to primary Bjerknes force [41]. At the same time a bubble near a wall will stick to that in clusters due to the secondary Bjerknes force [42]. The position of a MB near a wall changes the bubble response, signal amplitude is decreased [38]. GARBIN at al [43] motivated this behaviour through a change in resonance frequency of a bubble in presence of a wall and by non-spherical oscillations caused by non-symmetrical interaction of the bubble with the wall (see appendix A.6).

A.4 Acoustic bubble characterization

In an ensemble-averaged acoustic characterization the scattered pressure or pressure-time P-t-curve of the whole MB suspension is recorded. Through this the physical properties attenuation and phase velocity as described in appendix A.2 can be determined. This is relatively inexpensive and has the advantage of high sampling rate and great simplicity of the method itself [38]. However, the polydispersity of the MBs makes it difficult to relate the ensemble-averaged behaviour to the single bubble dynamics, since the acoustic response of a bubble strongly depends of its size and shell thickness [44]. To study the behaviour of a single bubble optical methods can be used that record the radial response of radius-time R-t-curve of a single bubble using f.ex. high-speed micrography [45]. The advantage is clearly that inspection of single bubbles is possible with high resolution and high accuracy [26]. The drawbacks are besides expensiveness that high frame rates are required to resolve MB oscillations in the MHz-range [23]. Another drawback is that the bubble needs to be attached to a membrane during data acquisition which leads to non-spherical oscillations (see appendix A.6.1). The presented work requires quick and easy characterization of the general MB suspension and acquisition of the MB

parameters shear modulus and shear viscosity, that is why acoustic characterization is used and further described in in the following.
By measuring the time-domain MB response to ultrasound exposure both attenuation and phase velocity can be determined. As reference a specimen filled with water is chosen. The signals are evaluated in frequency domain. To model the behaviour of a single bubble mostly the parameters shear modulus and viscosity of the coating are required. They can be acquired through fitting the measured curves to the theoretical model. [26]

A.4.1 Attenuation

Attenuation describes the reduction of the incident ultrasound wave energy when passing through a medium (see appendix A.2). In the linear range the attenuation coefficient is nearly independent of incident intensity whereas above a threshold it becomes proportional to the acoustic pressure [27]. It is frequency dependent and shows a maximum at resonance frequency (see appendix A.6). Below resonance frequency the attenuation curve shows Rayleigh scattering whereas above resonance attenuation decreases again and reaches a constant value [26]. The attenuation coefficient $\alpha(\omega)$ is achieved from

$$\alpha(\omega) = -\frac{20}{2L} \cdot log(\frac{|\hat{s}(\omega, L)|}{|\hat{s}_{ref}(\omega)|}) \qquad \text{[46] (A.4)}$$

with L being the thickness of the specimen, $\hat{s}$ and $\hat{s}_{ref}$ being the Fourier transformed measured signals. A simulated curve for an attenuation profile for single sized bubbles with diameter $3\,\mu\mathrm{m}$ presented by HOFF et al [14] is shown in fig. A.2.

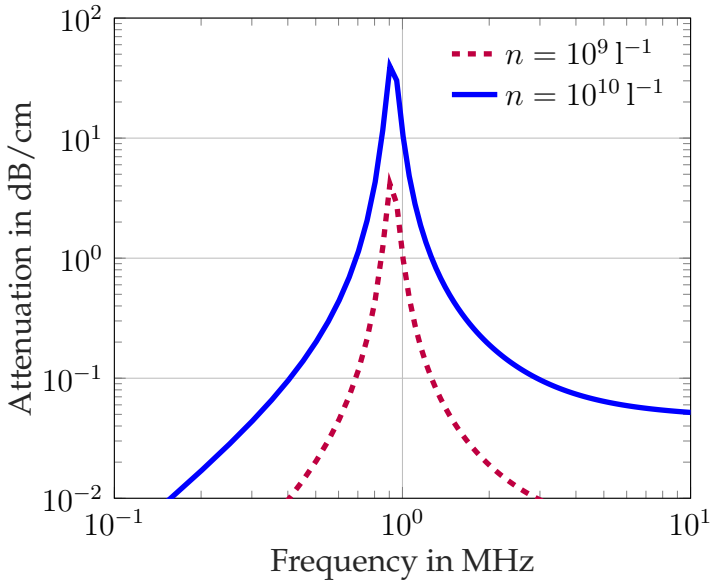

Figure A.2: Simulated attenuation curve for a bubble suspension with single sized bubbles of $3\,\mu\mathrm{m}$ diameter [14]

Due to the single sized bubble assumption a sharp resonance peak is visible. At higher concentration also the attenuation increases. In real MB suspension such as used in the presented work polydispersion causes a wider and flatter resonance peak in the attenuation profile.

A.4.2 Phase velocity

The simulated phase velocity for the single sized bubble solution is shown in fig. A.3.

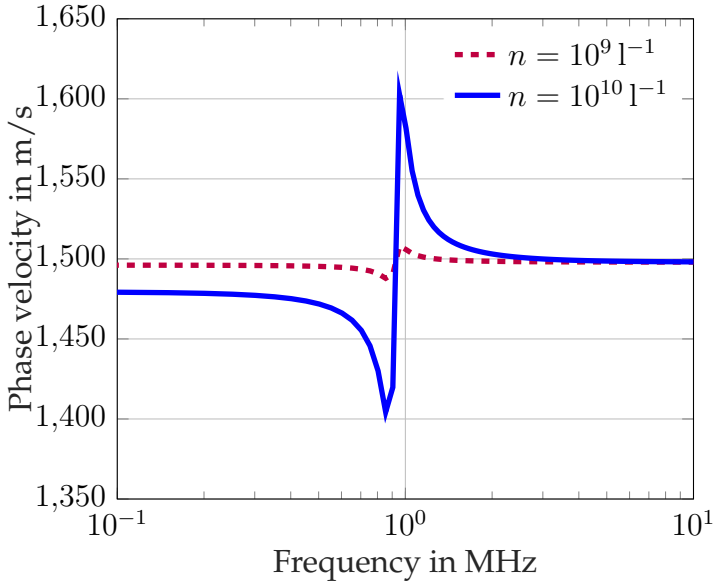

Figure A.3: Simulated phase velocity curve for a bubble suspension with single sized bubbles of $3\,\mu\mathrm{m}$ diameter [14]

However, the determination of phase velocity and dispersion is not trivial. Calculation of the phase angle in the FFT transformed signal is usually less accurate than that of the amplitude, introducing a large relative error in dispersion measurement when having small measurement uncertainties [33]. Also the magnitude of dispersion is usually small (<1 %), especially compared to the magnitude of attenuation [34]. Another problem are ambiguities in phase unwrapping and determination of the initial phase. Several approaches have been made to overcome the problems in phase velocity calculation:

- Naturally phase velocity is calculated from the phase difference between two pulses as for example GRISHENKOV [46] did:

$$\Delta\varphi = \varphi_{MB} - \varphi_{ref} = 2L \cdot \left(\frac{\omega}{c_{ref}} - \frac{\omega}{c(\omega)}\right) \tag{A.5}$$

  with φ_{MB} and φ_{ref} being the phase angle of the MB and reference solution and $c(\omega)$ and c_{ref} being the phase velocities in bubbly liquid and water, respectively. The equation then needs to be resolved for $c(\omega)$:

$$c(\omega) = \left(\frac{1}{c_{ref}} - \frac{\varphi_{MB} - \varphi_{ref}}{2L\omega}\right)^{-1} \tag{A.6}$$

- ZHAO et al [33] proposed an approach using short time Fourier transform (STFT) and time of flight (TOF). TOF is the difference of two successive times of arrival at two interfaces and can be used to determine speed of sound neglecting dispersion. Through determination of the TOF at monofrequencies also phase velocity can be calculated.

A.5 Theoretical description of the bubble behaviour

The Waterman and Truel condition says that the multiple scattering field caused by insertion of a bubble is much smaller than the field exciting that bubble [15]. This means that in sufficiently low concentration MBs can be treated as individual scatterers. In order to theoretically describe the dynamic behaviour of a given MB suspension individual bubble dynamics can be modeled and then superposed.
The behaviour of a single gas bubble under ultrasound pressure can be described theoretically by combining Bernouilli's equation and the continuity equation [5]. This was first done by LORD RAYLEIGH [47] and later redefined by several authors to consider surface tension and fluid viscosity (f.ex. by PLESSET [6]). In the following first the behaviour of a free gas bubble in liquid is described both non-linearly and linearized and CHURCH's model for coated bubbles is presented).

A.5.1 Modified Rayleigh-Plesset equation

Most commonly used to describe the behaviour of a free gas bubble in liquid is the modified Rayleigh-Plesset equation. Making the assumption that the bubble is surrounded by a liquid of infinite extend and constant viscosity, the bubble remains spherical during oscillation and that the bubble radius is small compared to the acoustic wavelength, the relation between radial motion and pressure difference at the liquid-gas interface are evaluated as follows:

$$\rho_L(\frac{3}{2}\dot{a}^2 + a\ddot{a}) = p_{int} - p_{ext} \qquad \text{[39] (A.7)}$$

with ρ_L being the density of the surrounding liquid and a, $\dot{a}$ and $\ddot{a}$ the bubble radius and its time derivatives velocity and acceleration of the bubble wall, respectively. p_{int} is the internal pressure that

contains both gas and capillary pressure. p_{ext} is the external pressure including ambient pressure p_0 and acoustic driving pressure p_i: $p_{ext} = p_0 + p_i$. This equation is a non-linear ordinary differential equation which leads to a non-linear relation between driving pressure p_i and radial oscillation a.

A.5.2 The microbubble as linear oscillator

If driving pressure is low and thus R shows small amplitude oscillations $x \ll 1$ then R can be approximated by

$$a = a_e \cdot (1 + \xi) \tag{A.8}$$

This leads to the linearized version of the Rayleigh-Plesset equation:

$$\ddot{\xi} + \omega_0 \delta \dot{\xi} + \omega_0^2 \xi = \frac{p_i}{\rho_L a_e^2} = F(t) \qquad \text{[23] (A.9)}$$

where $\omega_0 = 2\pi f_0$ is the eigenfrequency of the system and δ the damping coefficient. This is the equation of motion for a linear mechanical oscillator. The single MB can thus be seen as linear oscillator containing mass, spring and damping components. The mass represents the displaced liquid mass around the bubble, the spring considers the compressible gas [14]. Damping occurs through losses such as radiation, viscous damping or thermal damping [30]. The eigenfrequency f_0 of the system is the resonance frequency without damping. An estimate of the eigenfrequency has been done by MINNAERT [48]:

$$f_0 = \frac{1}{2\pi} \cdot \sqrt{\frac{3\kappa p_0}{\rho R_0^2}} \tag{A.10}$$

where κ is the polytropic exponent of gas inside the bubble which is usually $\kappa \approx 1.1$ for heavy gases. Assuming $\rho_L = 1000\,\frac{\mathrm{kg}}{\mathrm{m}^3}$ and $p_0 = 100\,\mathrm{kPa}$ the estimated bubble resonance is only dependent on the initial bubble radius:

$$f_0 a_e \approx 3\,\mu\mathrm{m} \cdot \mathrm{MHz} \tag{A.11}$$

The resonance frequency f_r of the whole system is a lowered compared to the eigenfrequency because of the damping by

$$f_r = f_0 \cdot \sqrt{1 - \frac{\delta^2}{2}} \qquad \text{[23] (A.12)}$$

However, this equation only holds true for a free or flexible coated gas bubble and only in the linear regime. When the bubble oscillations cross the so-called Blake threshold of $a_{max} > 2.2 \cdot a_e$ with a_{max} being the maximum bubble radius the linearized equations fail and the non-linear equation must be solved. [5]

A.5.3 Modeling of coated microbubbles

The above described model is only valid to describe uncoated or with adaptations flexible coated MBs. To describe the behaviour of rigid coated MBs several models exist, but no consensus on the best model to describe the details of the phenomena observed for MBs [30]. However, nearly all modeling approaches are Rayleigh-Plesset type models that additionally account for the shell by and effective surface tension $\sigma(R)$ and add a friction term F_r due to shell elasticity and viscosity [38]. Various models have been proposed by f.ex. DE JONG et al [49], HOFF et al [13], MARMOTTANT et al [8] or SARKAR et al [9]. Those models assume a viscoelastic thin shell and are thus not suitable to model the PVA coated MBs used in the presented work that have a shell thickness of ca 17 to 20 % of the bubble radius. The only existing model that does not make assumptions of the shell thickness is the one developed by CHURCH that is described in the following.

CHURCH's model suitable for thick shells

The model developed by CHURCH [11] is a Rayleigh-Plesset type equation that models the dynamics of bubbles with a shell of damped elastic solids. The estimated parameters for the shell description are the shear modulus G_S and shear viscosity η_S of the shell.
The basic assumption that is made is that the gas chore of the bubble is separated from the liquid by a solid, incompressible layer of finite shell thickness [38]. The liquid surrounding the bubbles is modeled as incompressible and Newtonian and surface tension can be neglected [14]. Under these assumptions the Rayleigh-Plesset equation can be modified to

$$\rho_L[\ddot{a}_2 a_2 + \frac{3}{2}\dot{a}_2^2] + \rho_s[\ddot{a}_2 a_2(\frac{a_2}{a_1} - 1) + \dot{a}_2^2(2\frac{a_2}{a_1} - \frac{1}{2}(\frac{a_2}{a_1})^4 - \frac{3}{2})]$$

$$= p_{g,0}(\frac{a_{1,0}}{a_1})^{3\kappa} - p_\infty(t) - 4\eta_L\frac{\dot{a}_2}{a_2} - 4\eta_S\frac{V_s}{a_2^3}\frac{\dot{a}_1}{a_1} - 4G_S\frac{V_s}{a_2^3}(1 - \frac{a_{1,0}}{a_1}) \quad \text{[11] (A.13)}$$

with $V_s = a_2^3 - a_1^3$, a_1 and a_2 are the inner and outer shell radii, respectively. $a_{1,e}$ and $a_{2,e}$ are the bubble radii at equilibrium, $p_{g,e}$ is the gas pressure in equilibrium and $p_\infty(t)$ is the pressure in liquid far away from the bubble. ρ_S and ρ_L are the densities of shell material and surrounding liquid. Further derivations of the equation can be read in [11].

A.6 Resonance frequency of microbubbles

Stimulating the UCA at resonance frequency is an important factor for ultrasound contrast imaging and therapeutic techniques and provides different advantages such as optimized conditions for generation acoustic radiation force [50]. Driven at resonance frequency MBs show maximum oscillation amplitude and therefore maximum attenuation and scattering. The resulting achievements are described by KOOIMAN et al [5] as follows:

- maximum interaction with cells
- maximum streaming potential and maximum shear stress
- maximum release of drugs when they are incorporated into the bubble construct
- maximum mixing of the bubble surrounding which introduces fresh samples for the medium into the region of interest

The resonant properties of UCA are mainly dependent on parameters of encapsulation and ambient medium [50]. Resonance frequency is defined as the frequency at which the amplitude of the bubble oscillation is maximum. At this frequency also the frequency dependent attenuation curve experiences a maximum (see appendix A.4.1). The resonance peak is sharpest for single-sized MB suspension. In real polydisperse populations only a subset of MBs will resonate at the driving frequency which causes a flatter maximum in the attenuation and oscillation profile [5]. To increase the bubble response in polydisperse suspension a frequency sweep signal or broad band signal can be used to activate a larger subset of MBs [51].

A.6.1 Types of bubble oscillations and their influence on the resonance frequency

A bubble can oscillate both spherically and non-spherically. The oscillation is called spherical or volumetric when the bubble keeps its spherical shape. Non-spherical oscillation is also called shape oscillation and occurs when the bubble changes its shape during the oscillation cycle. Non-spherical oscillation has an impact on the bubble response and the resonance frequency as explained in the following.

Spherical bubble oscillations

In an infinitively extended medium, at sufficiently low concentrations (10^{-4} to 10^{-6}) and at small oscillation amplitudes with relative excursion < 5 % MBs predominantly show spherical shape. In uncoated case the bubble can be modeled as linear oscillator (see appendix A.5.2). Following MARMOTTANT et al [52] the resonance frequency f_0 of the system has two contributions: the Minnaert frequency which is the eigenfrequency of the uncoated bubble (see eq. (A.10)) and a shell contribution.
For a linear oscillation the phase lag ϕ between the forcing term and the oscillator response is given as

$$tan(\phi) = \frac{\delta_{tot}}{\frac{f_r}{f} - \frac{f}{f_r}} \qquad \text{[23] (A.14)}$$

where δ_{tot} is the overall damping coefficient and f the driving frequency. The equation reveals that below resonance the oscillator is in phase with the driving force, insonification dominates. At resonance the oscillator response has a phase shift of $\frac{\pi}{2}$ to the driving force. Above resonance inertia dominate and the bubble response is out of phase with a phase shift of π [26].
In the approximation given by eq. (A.11) the resonance frequency of a $3\,\mu\mathrm{m}$ free gas bubble shrinks with increasing bubble radius and is $f_r \approx 1\,\mathrm{MHz}$. For a flexible coated MB f_r lies between 1 and $10\,\mathrm{MHz}$ which is also the range used for medical ultrasound imaging [16].
As explained in appendix A.5.3 the linear oscillator model is only valid for flexible coated bubbles. In rigid coating as used in the presented work the oscillatory dynamics of the bubble are dictated by the capsule properties and they usually provide much higher resonance frequencies [31].

Non-spherical bubble oscillations

According to BJERKNES et al [40] bubbles oscillating in phase have a net attractive force while bubbles oscillating out of phase repel each other. A MB near a rigid wall experiences a net attractive force towards the wall as its image bubble always oscillates in phase [38]. This effect caused by the second radiation force as explained in appendix A.3.3 is called Narcissus effect [52].
The presence of a rigid wall nearby a bubble can introduce non symmetrical shape deformations and microfluidic jets. VOS et al [53] observed large non-spherical deformations using an ultrasound field of $2.25\,\mathrm{MHz}$ center frequency and driving acoustic pressure between 80 to $325\,\mathrm{kPa}$ for C_4F_{10} filled MBs with phospholipid coating. He also showed that shape deformations generally have period-doubling effect and thus leads to subharmonic frequency components in the bubble response.
ZHAO ET AL [54] observed the oscillation of adherent MBs by high-speed photography and found that bubbles close to a boundary oscillate symmetrically in the plane parallel to the boundary and asymmetrically in the plane normal to the boundary in linear regime.
To describe non-spherical oscillations of free gas bubbles OVERVELDE et al [38] adapted the modified Rayleigh-Plesset by including the radiated pressure of the image bubble. Through linearisation it was found that in non-spherical oscillation the eigenfrequency of the bubble f_0^{wall} is reduced to

$$f_0^{wall} = \sqrt{\frac{2}{3}} f_0^{free} \tag{A.15}$$

with f_0^{free} being the eigenfrequency of a bubble in infinitely extended medium. Also it is shown by both [54] and [53] that shape deformations are most likely to occur at resonance frequency. The presence of a wall does thus have an impact on the oscillation characteristics and needs to be further explored.

Appendix B

Measures of Goodness

In the following the measures of goodness used in the fitting procedure are explained and their effects illustrated.

Mean squared error

The MSE is a commonly used measure to judge the quality of a fit. Main advantage in using the MSE as fitting criteria lies in its simplicity and intuitiveness, as well as in the fact, that it has a physical meaning [19]. To account for the frequency dependent sensitivity $sens$ the MSE is weighted

$$MSE_{weighted}(x, y) = \frac{1}{N} \sum_{i=1}^{N} (x_i - y_i)^2 \cdot P_{xx,i} \tag{B.1}$$

However, some disadvatages arise in the use of MSE as only measure. Mainly MSE compare the shape of two curves. The problem is presented in fig. B.1.

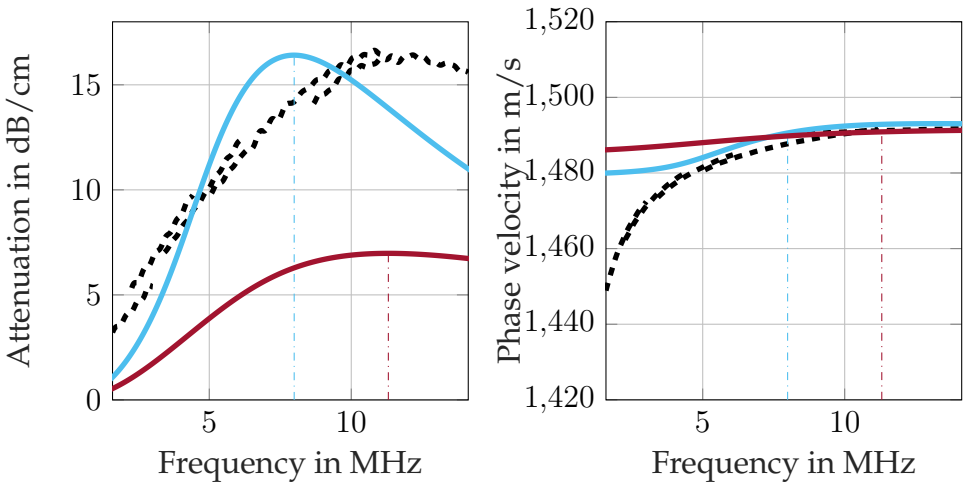

Figure B.1: Illustrating the usage of MSE as measure. Blue curve: $MSE = 5.3$, red curve: $MSE = 59.2$

The MSE in curve one is smaller than of curve two, but shape and in special resonance frequency of the experimental data are not met.

Cross-correlation

One solution to overcome the problem is to use the measure cross-correlation which is a measure of similarity between two signals and is given as

$$C = \frac{N \sum xy - \sum x \sum y}{\sqrt{(N(\sum x^2) - (\sum x)^2) \cdot (N(\sum y^2) - (\sum y)^2}} \tag{B.2}$$

for x,y,N as in the previous section. C can take values between -1 and 1. A cross-correlation of one means that the two signals are equal, a cross-correlation of zero means that they are uncorrelated. fig. B.2 illustrates the effect of using cross-correlation as measure to judge a fit.

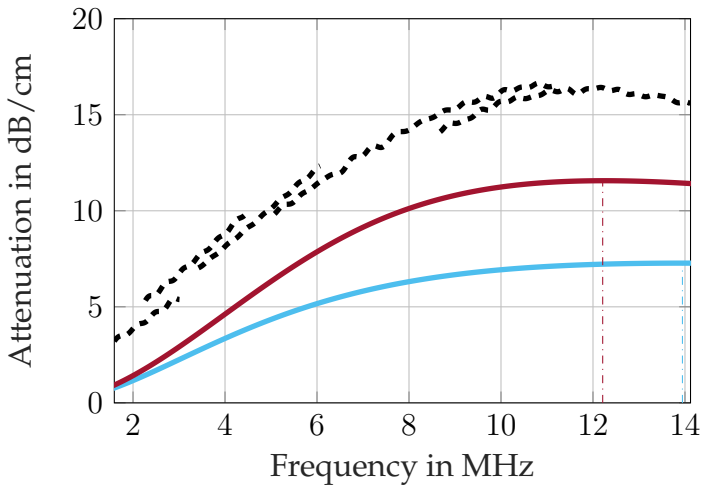

Figure B.2: Illustrating the usage of cross-correlation as measure. Blue curve: $C = 0.9946$, red curve: $C = 0.9949$

Both curves have similar cross-correlation coefficients. However, cross-correlation is apparently not able to judge the magnitude mismatch between two curves.

Position of Maximum

As additional refinement criteria it is considered especially important that maximum of experimental and simulated data match. Therefore the frequency difference Δf_r is introduced as measure:

$$\Delta f_r = |f(x_{max}) - f(y_{max})| \tag{B.3}$$

This measurement is only done for attenuation curve since in phase velocity is no specific feature to meet. Here also figure to illustrate.

TRITA CBH-GRU-2019:008